Capability of LCZ Scheme to Differentiate Urban Thermal Environments in Five Megacities of China: Implications for Integrating LCZ System Into Heat-Resilient Planning and Design

Bao-Jie He, Xuecheng Fu, Ziqi Zhao, Pengxin Chen, Ayyoob Sharifi, and Hong Li

***Abstract*—The local climate zone (LCZ) classification scheme provides a standardized method to characterize urban morphological characteristics and urban thermal environments. However, its capability to differentiate urban temperatures has not been well examined. This article investigated the LCZ-based land surface temperature (LST) in five megacities, including Shenyang, Beijing, Xi'an, Nanjing, and Nanchang. The results indicate that the LCZ scheme might conceal areas with the most critical heat risks, if the maximum LST was not used. The built-dominated zones often contributed to urban temperature increase, but it was not always true. The nonbuilt-dominated zones, mostly lowered urban temperatures, while they could contribute to urban temperature increase depending on seasonal and urban context. Both hot and cold nonbuilt-dominated zones varied significantly with city and season. Some zones were the hottest in one season, but changed to be the coldest in another season. LCZ scheme showed good capability to differentiate the temperatures of built-dominated zones, while its capability to characterize nonbuilt-dominated zones was weaker. In Beijing, the LCZ capability to characterize the temperature of nonbuilt-dominated zones was below 70%, and was only 16.67% in summer. Therefore, urban planners, designers, and managers should prudently adopt LCZ scheme to rank the priorities for integrating cooling interventions in both built-dominated and nonbuilt-dominated zones. It is important to not copy the LCZ-based LST pattern of other cities or seasons when making decisions. Overall, this article provides a reference to understand LCZ capability and make proper decisions for urban heat mitigation, adaptation, and management.**

***Index Terms*—Heat resilience, hot/cold zones, land surface temperature (LST), local climate zone (LCZ) capability, local climate zones (LCZs), seasonal variability.**

I. Introduction

THE world is currently under the mega threats of climate change at both global and local scales. Among various climate-related disasters, urban heat which is the individual or synergistic result of average temperature increase, heat waves, and heat islands has been evidenced as the most detrimental one [1], [2]. Addressing urban heat is a crucial mission to avoid cities being locked into unbearable heat-related challenges [3], [4]. Heat-resilient urban planning and design, a new paradigm aiming at increasing urban resilience to extreme heat by integrating heat mitigation, adaptation, and governance solutions into urban planning and design, has been proposed [5], [6]. The actual implementation of heat-resilient urban planning and design is highly dependent on the characterization of urban morphological characteristics [7], [8], [9]. For instance, heat-related threats and risks are a function of urban form and associated two-dimensional (2-D) and 3-D geometric and functional factors [10], [11], [12]. The determination of strategies for mitigation also depends on planning and design variables of roads, buildings, and open spaces [13], [14]. The regulation of wind and shade to enhance urban cool sources and weaken heat sources is also dependent on urban form and morphological characteristics, such as building height, building density, street aspect ratio, sky view factor, and street sinuosity [15], [16], [17], [18], [19].

Many studies have been carried out to characterize urban form and physiomorphological characteristics and to explore the relationship between urban form and urban thermal environments

Received 4 July 2024; revised 26 August 2024; accepted 23 September 2024. Date of publication 26 September 2024; date of current version 23 October 2024. This work was supported in part by the National Natural Science Foundation of China under Grant 42301339 and Grant 32101337; in part by the Fundamental Research Funds for the Central Universities under Grant 2024CDJXY014; in part by the China Meteorological Administration Youth Innovation Team Project under Grant CMA2024QN15; and in part by the Joint Open Fund Project of Shenyang Institute of Atmospheric Environment, China Meteorological Administration under Grant 2023SYIAEKFMS02. *(Corresponding author: Hong Li.)*

Bao-Jie He is with the Key Laboratory of New Technology for Construction of Cities in Mountain Area, School of Architecture and Urban Planning, Ministry of Education, Chongqing University, Chongqing 400045, China, also with the Institute for Smart City of Chongqing University in Liyang, Chongqing University, Liyang 213300, China, also with the School of Architecture, Design and Planning, The University of Queensland, Brisbane, QLD 4072, Australia, and also with the CMA Key Open Laboratory of Transforming Climate Resources to Economy, Chongqing 401147, China.

Xuecheng Fu is with the School of Architecture and Urban Planning, Ministry of Education, Chongqing University, Chongqing 400045, China, and also with the Institute for Smart City of Chongqing University in Liyang, Chongqing University, Liyang 213300, China.

Ziqi Zhao is with the Institute of Atmospheric Environment, China Meteorological Administration, Shenyang 110166, China.

Pengxin Chen is with the Shenyang Meteorological Service, Shenyang 110001, China.

Ayyoob Sharifi is with the The IDEC Institute, Hiroshima University, Hiroshima 739-0046, Japan, and also with the School of Architecture and Design, Lebanese American University, Beirut 03797751, Lebanon.

Hong Li is with the School of Architecture and Urban Planning, Ministry of Education, Chongqing University, Chongqing 400045, China, and also with the Key Laboratory of New Technology for Construction of Cities in Mountain Area, Ministry of Education, Chongqing University, Chongqing 400045, China (e-mail: lihom@cqu.edu.cn).

Digital Object Identifier 10.1109/JSTARS.2024.3469241

[20], [21]. For instance, the characterization of land use/land cover has acquired wide acceptance in explaining surface-based thermal environments [22], [23]. In summer, buildings and roads are often characterized as hotspots, while water bodies and vegetated zones are mostly distinguished as cold spots [24], [25]. Moreover, local climate zone (LCZ) scheme was developed to standardize local morphological characteristics and to differentiate urban temperatures and heat vulnerability of different local areas [26], [27]. Given its advantages in clustering homogeneous zones and differentiating heterogeneous zones, urban planners, designers, and managers can easily identify heat-prone zones and make decisions on heat mitigation, adaptation, and governance [28], [29], [30]. The application of LCZ scheme is conducive to transform heat-related sciences and technologies into heat-resilient planning and design practices. However, with in-depth understandings of LCZ-related urban temperatures, many studies have revealed different results from the classic temperature patterns, resulting in doubts about the LCZ scheme's robustness and capability, as well as the suitability of integrating LCZ scheme into heat-resilient planning and design. For instance, through the empirical investigation in Prague, Brno, and Novi Sad, Geletič et al. [31] concluded that each LCZ class and subclass exhibited seasonal variability, and many pairwise LCZ types showed no significant temperature differences. Zhao et al. [32] carried out a holistic assessment of pairwise difference of monthly temperatures in Shenyang, China. Their results indicate that the pairwise built-dominated zones with significant differences accounted for 80.0%–93.3% across 12 months, where the LCZ capability to differentiate urban temperature was the strongest in summer, but the lowest in transition months; in rural areas, the capability ranged between 33.3% (September) and 88.9% (July) for built-dominated zones, while between 57.1% (September) and 95.2% (July and August) for nonbuilt-dominated zones [32]. Another study in four inland and five coastal cities in Croatia verified insignificant temperature differences among many pairwise LCZ zones [33].

Overall, the LCZ scheme's capability to differentiate urban temperatures varies seasonally and temporally. This lays a trap for urban planners, designers, and managers to apply the LCZ scheme, mainly in aspect of underestimating or overestimating urban temperatures of specific zones in different seasons and areas. To avoid inaccurate information and biased decisions, it is essential to determine in which season the LCZ capability is the most robust, and vice versa. However, the understanding of LCZ scheme's capability is still limited. Therefore, this article aims to deal with this research gap by investigating the capability of the LCZ scheme to differentiate urban thermal environments in five China megacities. These cities include Shenyang, Beijing, Xi'an, Nanjing, and Shanghai from the northern to the southern part of China. The seasonal variation of LCZ-based land surface temperature (LST) and LCZ capability are investigated. This article is expected to provide an empirical understanding of LCZ scheme's capability to differentiate urban thermal environments and to offer a reference for urban planners, designers, and managers to accurately characterize hot and cold zones for performing unbiased heat-resilient urban planning and design.

II. Study Area and Methodology

A. Study Area

This article was carried out in five megacities including Shenyang (41 °48'N, 123 °23'E), Beijing (39 °55'N, 116 °25'E), Xi'an (34 °16'N, 108 °57'E), Nanjing (32 °3'N, 118 °47'E), and Nanchang (28 °41'N, 115 °54'E) in China (Fig. 1). Shenyang, Xi'an, Nanjing, and Nanchang are the capital cities of Liaoning, Shaanxi, Jiangsu, and Jiangxi Province, respectively. From the north to south, these five cities range from 41 °48' N to 28 °41'N. They have different distances from the coastal areas, where Xi'an and Nanchang are inland cities, while Shenyang, Beijing, and Nanjing can be potentially affected by sea breeze. These five cities have different altitudes, where the average elevations of Shenyang, Beijing, Xi'an, Nanjing, and Nanchang are 41.6, 50.0, 396.6, 67.9, and 25.0 m, respectively.

All cities are characterized by different climates. Shenyang has a monsoon-influenced humid continental climate (Dwa), with four distinct seasons. Beijing has a monsoon-influenced humid continental climate (Dwa), but it borders on a cold semi-arid climate (BSk). Xi'an has a combined climate of semiarid climate (BSk) and humid subtropical climate (Cwa), with four distinct seasons. Nanjing has a humid subtropical climate (Cfa), with four distinct seasons. Nanchang has a monsoon-influenced humid subtropical climate (Cfa) with four distinct seasons. It is also on the list of furnace cities of China due to its hot and humid summers. During its hot season (June 10–September 17), the average daily high temperatures ranged between 29 °C and 34 °C. Annually, the days of a maximum temperature above 32 °C reach 66 days.

These five cities are highly urbanized. First, these cities have large populations. As of 2023, Shenyang, Beijing, Xi'an, Nanjing, and Nanchang were home to 9.20 million, 21.85 million, 13.07 million, 9.54 million, and 6.57 million, respectively. Second, the urbanization levels of these five megacities were 85.12%, 87.80%, 79.88%, 87.20%, and 79.58%, respectively, much higher than the national urbanization level of China (66.2%). However, the high urbanization levels, associated with little attention to cool source preservation and heat source mitigation, have brought heat islands to these cities.

Subject to climate change, all cities are undergoing extreme climates. For instance, Shenyang saw an extreme temperature of 39.3 °C on 2 August 2018. Beijing broke a 23-year record with 27 consecutive days of temperature above 35 °C in July 2023. Xi'an saw a new temperature record of 40 °C on 28 July 2019. Nanjing suffered an extreme temperature of 39 °C on 28 July 2019, and the extreme temperature of Nanchang was 40 °C on 28 July 2019. Overall, owning to heat islands and climate change, the urban heat challenges are increasingly intense, making it more pressing to implement heat-resilient urban planning and design.

B. Data Preprocessing and Date Selection

The LST data of the five megacities were retrieved from Landsat 8 images. In order to reveal the seasonal variability of LST, SUHI, LCZ-based LST, and LCZ scheme's capability, a

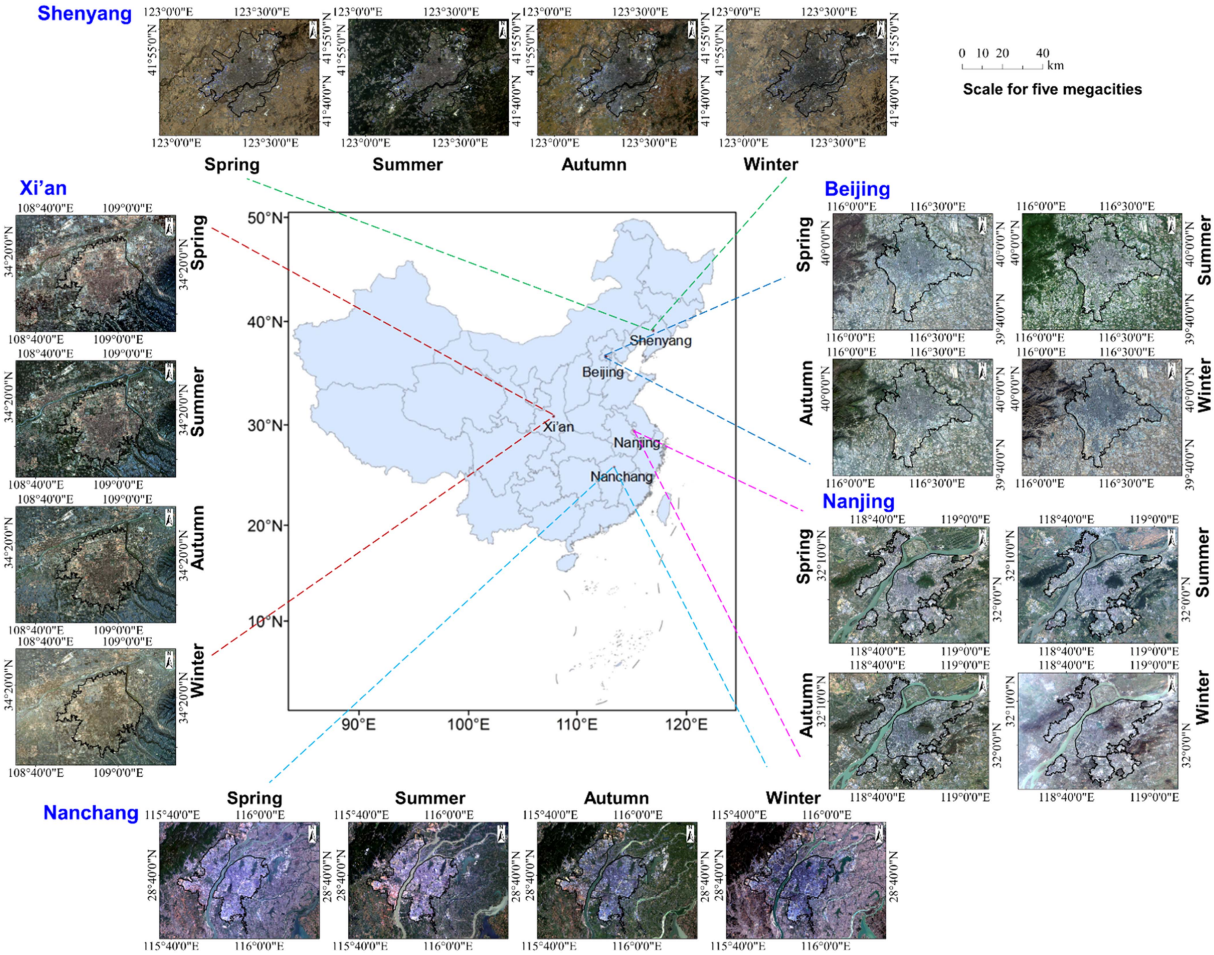

Fig. 1. Locations of the five megacities and seasonal land composition in which the black buffer in the year of 2018 is provided by the resource and environmental science data platform (http://www.resdc.cn).

thermal image in each season was prepared for all the megacities. A total of 20 remotely sensed thermal-infrared images with a resolution of 30 m were obtained from the U.S. Geological Survey (http://earthexplorer.usgs.gov). The cloud coverage was strictly controlled below 1.0% to avoid errors. The date of each image adopted to represent each season and the specific time of thermal information in a day are given in Table I. It should be noted that it is favorable to control all date in the same year for comparison, while the cloud condition is often a prominent constraint. On the basis of thermal images in 2019 and 2020, we searched satisfactory thermal images in a reverse order from 2018 to achieve effective supplementation. Other meteorological variables (e.g., air temperature and relative humidity) at 10:28–11:20 (local time) were collected from the local meteorological departments (Table I). Air temperature data of all five megacities verified the consistency of seasonal temperature changes.

C. Landsat Image Processing and LST Retrieval

The LST retrieval followed a common process. After atmospheric correction of reflective and thermal bands, the LST was retrieved based on the split window algorithm from the only spectral band of thermal-infrared sensor (TIRS) 10 in Landsat 8 [24], [32]. The digital number was converted to the spectral radiance L_λ at the top of the atmosphere as

$$L_\lambda = M_L \cdot DN + A_L \tag{1}$$

where L_λ is spectral radiance, $\mathrm{W}/(\mathrm{m}^2\mathrm{sr}\mu\mathrm{m})$; M_L is the rescaled gain corresponding to a specific band, $\mathrm{W}/(\mathrm{m}^2\mathrm{sr}\mu\mathrm{m})$; and A_L is the rescaled bias corresponding to a specific band, $\mathrm{W}/(\mathrm{m}^2\mathrm{sr}\mu\mathrm{m})$.

At-sensor brightness temperature was calculated from TIRS 10, corresponding to the OLI sensor, based on

$$T_b = k_2 \,/\, (\ln(k_1/L_\lambda) + 1) \tag{2}$$

where T_b at-sensor brightness temperature, K; k_1 is a constant, $\mathrm{W}/(\mathrm{m}^2\mathrm{sr}\mu\mathrm{m})$, with a value of 774.89; and k_2 is a constant, W, with a value of 1321.08.

Next, based on the following equations, the LST was received after emissivity correction of ground radiance via mono window

TABLE I
DETAILS OF THE DATE, TIME, AND CORRESPONDING METEOROLOGICAL VARIABLES OF 20 THERMAL-INFRARED IMAGES

Megacities	Path/ row	ID	Seasons	Date	Local time	Air temperature/℃	Relative humidity/%
Shenyang	119, 31	1	Spring	2020-04-01	10:28	8.4	21
		2	Summer	2020-07-22	10:28	28.9	58
		3	Autumn	2020-10-10	10:28	19.1	53
		4	Winter	2019-01-09	10:28	–7.7	38
Beijing	123, 32	5	Spring	2020-04-13	10:53	15.8	54
		6	Summer	2017-07-10	10:53	32.3	45
		7	Autumn	2019-10-20	10:53	22.4	63
		8	Winter	2020-12-25	10:53	–0.7	32
Xi'an	127, 36	9	Spring	2020-04-09	11:19	18.0	48
		10	Summer	2019-08-13	11:19	28.0	56
		11	Autumn	2018-10-29	11:20	14.8	39
		12	Winter	2019-01-17	11:20	–2.7	56
Nanjing	120, 38	13	Spring	2019-04-06	10:36	20.8	55
		14	Summer	2018-06-06	10:36	27.2	55
		15	Autumn	2019-10-31	10:37	20.6	40
		16	Winter	2020-01-19	10:37	5.3	73
Nanchang	121, 40	17	Spring	2020-04-15	10:43	19.5	57
		18	Summer	2016-06-23	10:44	33.1	63
		19	Autumn	2018-10-03	10:44	24.7	40
		20	Winter	2021-01-12	10:44	3.6	45

algorithm:

$$B\,(\mathrm{LST}) = \{a\,(1-C-D)+[(-1)\,(1-C-D)+1]\,T_b - DT_a\}\,/C \tag{3}$$

$$C = \varepsilon\tau \tag{4}$$

$$D = (1-\varepsilon)\,[1+(1-\varepsilon)\,\tau] \tag{5}$$

$$\mathrm{LST} = B\,(\mathrm{LST})\,/(\ln\varepsilon\ (\lambda\cdot B\,(\mathrm{LST})\,/\rho+\ 1) \tag{6}$$

where B(LST) is the ground radiance, K; a and b are constants; and ε and τ are land surface emissivity and atmospheric transmittance of band i, respectively. T_a is effective mean atmospheric temperature, K. λ is the wavelength of emitted radiance (11.5 μm). ρ is a constant calculated by Planck's constant, light velocity, and Boltzmann's constant, $m\cdot K$, with a value of 1.438×10^{-2}.

Based on (7), the effective mean atmospheric temperature was calculated.

For mid-latitude summer

$$T_a = 16.0110 + 0.92621\,T_0. \tag{7}$$

For mid-latitude winter

$$T_a = 19.2704 + 0.91118\,T_0$$

where T_a is the effective mean atmospheric temperature, K; and T_0 is the air temperature at the time when Landsat images are photographed, K.

A remote sensing image can be divided into three types of underlaying surfaces, such as water, urban, and natural surfaces. The land surface emissivity ε of water, urban, and natural surfaces were represented by $\varepsilon_{\mathrm{water}}$, $\varepsilon_{\mathrm{building}}$, and $\varepsilon_{\mathrm{surface}}$ as follows:

$$\begin{aligned}\varepsilon_{\mathrm{water}} &= 0.995\\ \varepsilon_{\mathrm{building}} &= 0.9589+0.0860\times F_v-0.0671\times {F_v}^2\\ \varepsilon_{\mathrm{surface}} &= 0.9625+0.0614\times F_v-0.0461\times {F_v}^2\end{aligned} \tag{8}$$

where F_v is the fractional vegetation cover, calculated based on

$$F_v = \frac{\mathrm{NDVI}-\mathrm{NDVI}_s}{\mathrm{NDVI}_v-\mathrm{NDVI}_s} \tag{9}$$

where the NDVI is the normalized difference vegetation index, as expressed by (10), and NDVI_s and $\mathrm{NDVI}_v$are the NDVI indexes for soil and vegetation, respectively [34]. NDVI_s and NDVI_v are set as 0.05 and 0.70, while the F_v is set as 1.0 when the NDVI of a pixel exceeds 0.70, and set as 0 when the NDVI of a pixel is below 0.05

$$\mathrm{NDVI} = \frac{L_{\mathrm{NIR}}-L_R}{L_{\mathrm{NIR}}+L_R} \tag{10}$$

where L_{NIR} is the reflectance in the NIR region and L_R refers to the reflectance in the red region [35].

D. Local Climate Zone (LCZ) Map Generation

The WUDAPT platform (https://www.wudapt.org/) offers a portal with tools to standardize the generation of LCZs in cities. The LCZs of many cities are accessible, where we obtained the LCZ maps of Shenyang, Beijing, Xi'an, and Nanjing [36] in 2019 (Fig. 2), while the LCZ map of Nanchang was not available.

Therefore, we generated the LCZ map of Nanchang following the criteria and principles specified by Stewart et al. [26]. Based on the Google Earth image on 15 April 2020 (no cloud), the visual interpretation was conducted to select training LCZ

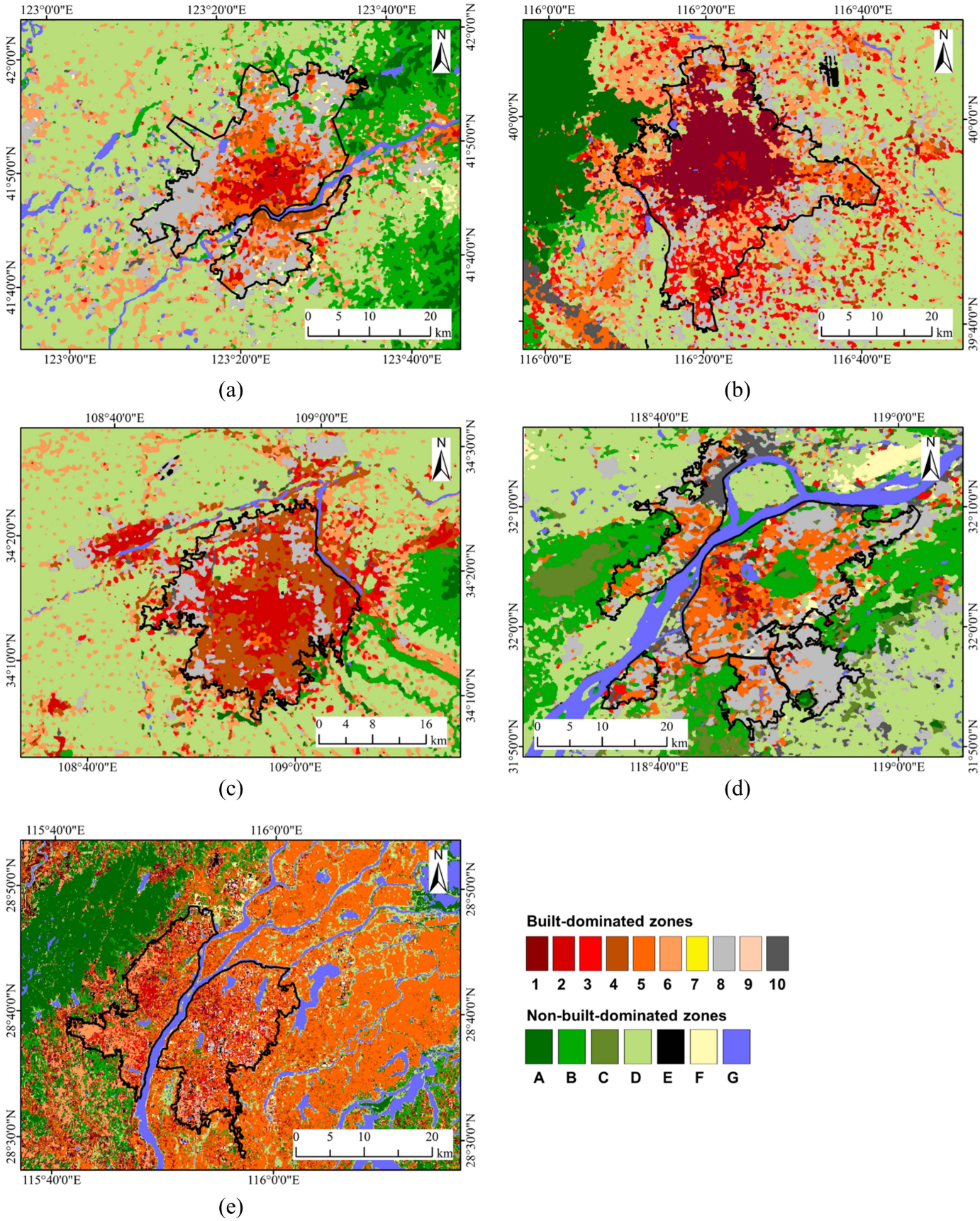

Fig. 2. Local climate zone maps of five megacities. (a) Shenyang. (b) Beijing. (c) Xi'an. (d) Nanjing. (e) Nanchang.

TABLE II
AREAS OF DIFFERENT LCZ TYPES URBAN BUILT-UP AREAS OF FIVE MEGACITIES

LCZ types	Built-up area (km^2)				
	Shenyang	Beijing	Xi'an	Nanjing	Nanchang
LCZ-1 (compact high-rise)	9.79	379.84	0.01	8.82	41.93
LCZ-2 (compact midrise)	75.59	63.33	134.74	22.48	40.75
LCZ-3 (compact low-rise)	16.77	108.56	51.12	10.31	32.28
LCZ-4 (open high-rise)	40.91	19.96	215.20	37.42	38.10
LCZ-5 (open midrise)	144.23	83.28	5.18	179.56	153.49
LCZ-6 (open low-rise)	74.96	136.47	13.21	23.95	66.23
LCZ-7 (lightweight low-rise)	–	–	–	–	–
LCZ-8 (large low-rise)	252.47	164.13	103.06	263.08	12.34
LCZ-9 (sparsely built)	–	–	–	–	–
LCZ-10 (heavy industry)	3.01	1.48	7.52	53.59	–
LCZ-A (dense trees)	0.66	0.32	0.39	9.37	6.38
LCZ-B (scattered trees)	38.37	–	0.29	48.42	4.92
LCZ-C (bush, scrub)	–	–	–	7.72	3.10
LCZ-D (low plants)	36.72	79.81	35.01	35.25	10.33
LCZ-E (bare rock or paved)	0.11	0.05	0.52	2.26	21.77
LCZ-F (bare soil or sand)	13.96	–	–	5.60	15.77
LCZ-G (water)	6.04	2.90	0.40	10.06	16.89

samples. To ensure training efficiency, some criteria were set as follows.

1) Each training sample was required to be larger than 1.0 sq km and longer/wider than 200 m.
2) Small areas that are highly heterogeneous or irregular in morphological characteristics are excluded.
3) The distance between two training zones should be wider than 100 m to avoid fuzzy recognition.

Depending on the availability, 5–28 training samples were selected for each type. Using the random forest algorithm on the SAGA GIS platform, the initial LCZ training samples were classified, after which LCZ map was generated on the Landsat TM image. Through several rounds of iteration and verification, the final LCZ map of Nanchang was generated, as shown in Fig. 2(e). Detailed information of each LCZ type of five megacities is provided (Table II). Note that not all types were available in each megacity. For instance, LCZ-7 (lightweight low-rise) and LCZ-9 (sparsely built) were not available in all megacities, LCZ-10 (heavy industry) was not found in Nanchang. LCZ-B (scattered trees) was not found in Beijing, LCZ-C (bush and scrub) was not available in Shenyang, Beijing, and Xi'an, and LCZ-F (bare soil or sand) was not found in Beijing and Xi'an. In addition, LCZ-1 (compact high-rise) in Xi'an only had an area of 0.01 sq km.

E. Data Analysis

The seasonal LST of different LCZs were calculated within the urban built-up areas (circled by black lines in Fig. 2). The analysis was carried out in terms of LST range, mean value, and departure of the average LST of a specific LCZ from the average LST of all LCZs, in order to test whether a zone has positive or negative impacts on urban temperature. Afterwards, the LCZ scheme's capability to differentiate LST was examined by examining if there were significant differences between the LSTs of pairwise LCZs based on the nonparametric analysis of Kruskal–Wallis H test because the LST dataset did not obey a normal distribution [2]. The capacity was defined as the ratio of significantly different pairwise LCZs to all pairwise LCZs, with a range of 0%−100%, in built-dominated and nonbuilt-dominated areas, respectively.

III. RESULTS AND DISCUSSION

This section presents the seasonal variability of LCZ-based LSTs and their departure from the average temperature of each megacity to examine each zone's contribution to the urban thermal environments. Afterwards, the seasonal variability of hot and cold zones of each megacity was examined in terms of the hottest and coldest built-dominated and nonbuilt-dominated zones. The LST difference of pairwise LCZs was analyzed to reveal whether the LCZ scheme could differentiate LST robustly.

A. Seasonal Variability of LCZ-Based LST in Shenyang

The summertime LST of Shenyang ranged between 12.71 °C and 45.32 °C (Fig. 3). Moreover, the autumntime, wintertime, and springtime ones ranged between 5.78 °C–29.46 °C, −28.50 °C–1.72 °C, and −2.15 °C–30.99 °C, respectively. The two ends of the range in each season were taken by LCZ-8, showing a large range of 32.61 °C, 23.68 °C, 30.22 °C, and 32.14 °C in summer, autumn, winter, and spring, respectively. Using the average LCZ-based LST as an indicator, the summertime LST ranged between 27.80 °C (LCZ-A) and 34.79 °C (LCZ-2), showing a range of 6.99 °C. The autumntime LST ranged between 18.51 °C (LCZ-G) and 21.77 °C (LCZ-8), showing a range of 3.26 °C. The wintertime LST ranged between −7.76 °C (LCZ-4) and −4.53 °C (LCZ-D). The springtime LST ranged between 14.18 °C (LCZ-G) and 19.53 °C (LCZ-8), presenting a range of 5.35 °C. Overall, in summer, the dense tree areas were important cooling sources for the city. Meanwhile, the hot and cold areas varied with the change of temperature assessment indicator. The highest and lowest temperatures could be masked and the temperature gaps were reduced by the use of average LST when introducing LCZ scheme.

Fig. 4 shows the departure of average LST of each LCZ zone from the citywide average temperatures. In summer, the

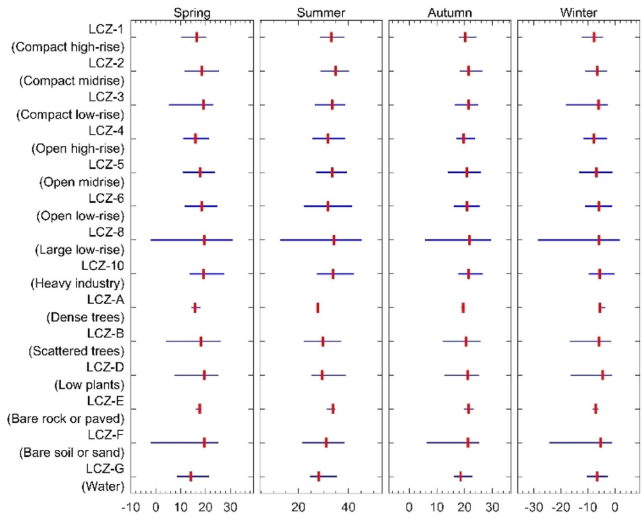

Fig. 3. Seasonal LST of different LCZs in Shenyang (°C). Note that the red dot was the average LST of each zone, and the left and right ends of the blue lines were the lowest and highest LSTs of each zone, respectively.

citywide average temperature was 31.90 °C. Seven LCZs exhibited higher temperatures, where LCZ-2 showed the largest positive departure (2.89 °C), followed by LCZ-8 (2.34 °C) and LCZ-10 (1.86 °C). LCZ-1, LCZ-3, LCZ-5, and LCZ-E also showed positive departure. Seven LCZs exhibited lower temperatures, where LCZ-4 and LCZ-6 were the built-dominated zones showing marginally negative departure. All others were nonbuilt-dominated zones, where LCZ-A and LCZ-G showed strong negative departure of 4.10 °C and 3.72 °C, respectively. In autumn, LCZ-1 and LCZ-4 were the built-dominated zones having lower temperatures than the citywide LST (20.71 °C). LCZ-A, LCZ-B, and LCZ-G were nonbuilt-dominated zones showing negative departure, about 1.25 °C, 0.25 °C, and 2.20 °C, respectively. However, LCZ-D, LCZ-E, and LCZ-F showed positive departure. In winter, four built-dominated zones showed negative departure, where the negative departure of LCZ-1 and LCZ-4 was 1.40 °C and 1.49 °C, respectively. LCZ-A, LCZ-B, LCZ-D, and LCZ-F were nonbuilt-dominated zones showing positive departure, where LCZ-D showed the largest departure of 1.74 °C. Only LCZ-E and LCZ-G showed negative departure. The springtime average citywide LST was 17.83 °C, and the springtime departure pattern was similar to the autumntime one. LCZ-5 showed a different pattern with a marginally negative departure (−0.02 °C). LCZ-B and LCZ-E showed different patterns with the values of 0.32 °C and 0.16 °C, respectively. Overall, LCZ-3, LCZ-8, and LCZ-10 were stable heating sources, while LCZ-G was a stable cooling source.

B. Seasonal Variability of LCZ-Based LST in Beijing

Fig. 5 exhibits the mimumin, average, and maximum LST of each LCZ in Beijing. Its summertime LST ranged between 24.09 °C and 53.95 °C, showing a range of 29.86 °C. However, the autumntime, wintertime, and springtime LST ranged between 5.23 °C–28.42 °C, −11.20 °C–9.50 °C, and 11.32 °C–44.12 °C, with a range of 23.19 °C, 20.70 °C, and 32.80 °C, respectively. The lowest and highest ends varied in different seasons, where they were LCZ-1 and LCZ-8 in summer, LCZ-8 and LCZ-8 in autumn, LCZ-1 and LCZ-8 in winter, and LCZ-1 and LCZ-8 in winter. However, the average LST ranged between 30.86 °C (LCZ-G) and 42.66 °C (LCZ-2) in summer, showing a range of 11.80 °C. In autumn, the average LST ranged between 15.99 °C (LCZ-G) and 21.09 °C (LCZ-2), having a range of 5.10 °C. In winter, the average LST ranged between −0.17 °C (LCZ-G) and 3.08 °C (LCZ-D), with a range of 3.25 °C. In spring, the average LST ranged between 20.24 °C (LCZ-G) and 31.99 °C (LCZ-3), with a range of 11.75 °C. The results also verified that different assessment indicators resulted in distinct zones with the highest and lowest temperatures.

Fig. 6 analyzes the departure of average LST of each zone from citywide average temperatures. In summer, the citywide average LST was 38.71 °C. LCZ-4 and LCZ-6 were the two built-dominated zones showing negative departure. All others positively contributed to urban temperature increase. LCZ-2 and LCZ-10 made the strongest contributions by 3.95 °C and 2.79 °C, respectively. Three out of four nonbuilt-dominated zones showed negative departure, where LCZ-A and LCZ-G showed large negative departure, 4.25 °C and 7.85 °C, respectively. In autumn, the citywide average LST was 19.83 °C. LCZ-4 was the only built-dominated zone showed negative departure (0.92 °C), while LCZ-2, LCZ-3, and LCZ-10 exhibited positive departure, with a value of 1.26 °C, 1.11 °C, and 1.14 °C, respectively. LCZ-D showed positive departure (0.38 °C), while LCZ-A, LCZ-E, and LCZ-G showed negative departure, with a value of 0.20 °C, 0.76 °C, and 3.84 °C, respectively. In winter, five built-dominated zones showed positive departure, while three showed negative departure. The most prominent negative departure (1.55 °C) was in LCZ-4. Two nonbuilt-dominated zones, including LCZ-A and LCZ-D, showed positive departure, where LCZ-D showed the most obvious departure of 1.46 °C. LCZ-E and LCZ-G showed negative departure. The springtime departure pattern was similar to the autumntime one, despite some variations in departure distance. Overall, LCZ-2, LCZ-3, LCZ-8, and LCZ-10 were the stable warming zone, while LCZ-G was the stable cool source. However, it is essential to notice the changing contributions of many other zones.

C. Seasonal Variability of LCZ-Based LST in Xi'an

Fig. 7 shows the minimum, average, and maximum LST of each zone in Xi'an. Summertime, autumntime, wintertime, and springtime citywide LST ranged between 22.80 °C–49.05 °C, 1.92 °C–36.12 °C, −1.27 °C–14.25 °C, and 18.91 °C–43.15 °C, with a range of 26.25 °C, 34.20 °C, 15.52 °C, and 24.24 °C, respectively. The two ends were LCZ-8 and LCZ-8 in summer, LCZ-8 and LCZ-8 in autumn, LCZ-8 and LCZ-8 in winter, and LCZ-G and LCZ-8 in spring. The summertime average LST ranged from 30.42 °C to 37.61 °C, with the lowest temperature shifting to LCZ-G. In autumn, the lowest average LST was in LCZ-G (19.34 °C), while the highest was in LCZ-A (26.04 °C). In winter, LCZ-4 showed the lowest average LST (3.03 °C), while LCZ-A was the one exhibiting the highest average LST (6.95 °C). In spring, the lowest average LST was found in

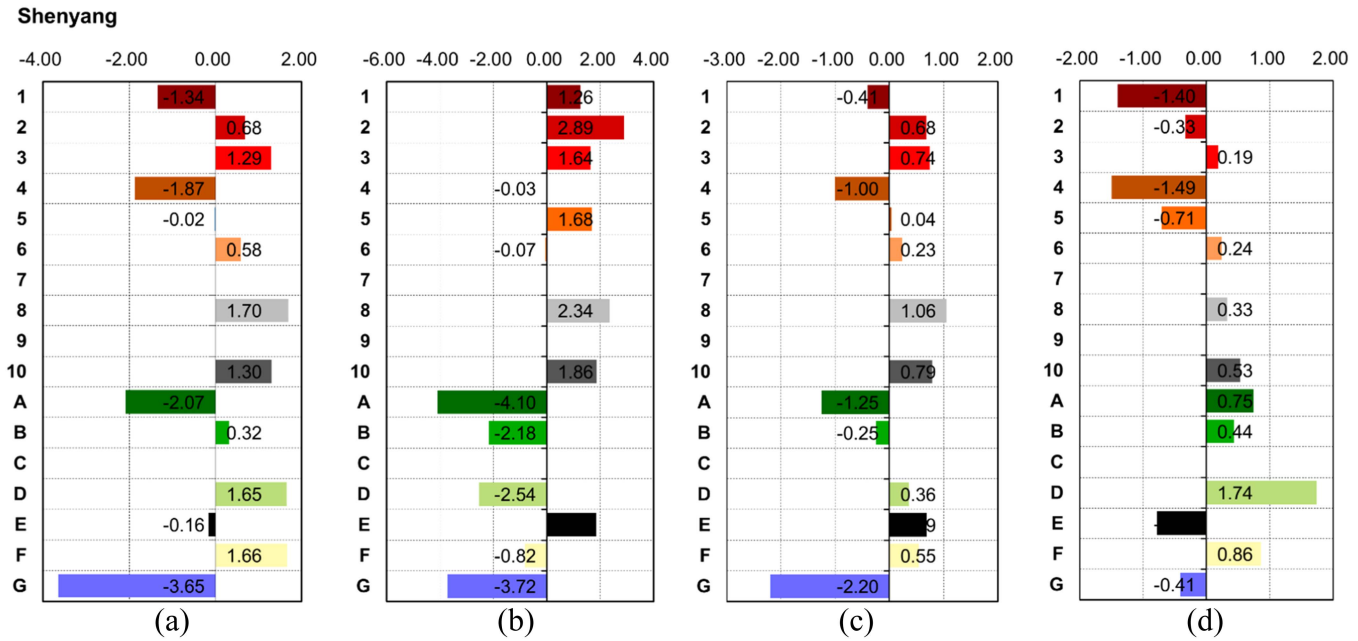

Fig. 4. Departure of LCZ-based LST from the average citywide LST in Shenyang. (a) Spring. (b) Summer. (c) Autumn. (d) Winter.

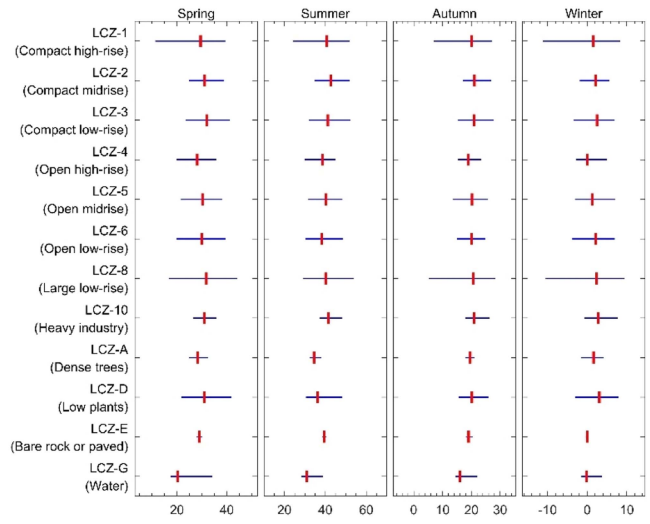

Fig. 5. Seasonal LST of different LCZs in Beijing (°C). Note that the red dot was the average LST of each zone, and the left and right ends of the blue lines were the lowest and highest LSTs of each zone, respectively.

LCZ-G (23.83 °C), but the highest average LST was found in LCZ-A (29.96 °C). Zones with the lowest/highest LST and lowest/highest average LST could be different and vary with season.

Fig. 8 shows the departure of average LST of each zone from citywide average temperatures. In summer, the citywide average LST was 34.52 °C. LCZ-4 and LCZ-6 were the two built-dominated zones having prominent negative departure, with value of 1.02 °C and 1.29 °C, respectively. LCZ-1 and LCZ-8 showed obvious positive departure of 2.80 °C and 1.49 °C, followed by LCZ-2 (0.72 °C), LCZ-5 (0.59 °C), and LCZ-3 (0.47 °C). Three nonbuilt-dominated zones showed negative departure. They were LCZ-G (4.10 °C), LCZ-A (3.00 °C), and LCZ-D (0.85 °C). LCZ-E showed positive departure, about 1.16 °C. In autumn, the citywide average LST was 21.95 °C. LCZ-1, LCZ-2, LCZ-4, and LCZ-5 showed negative departure, while LCZ-3, LCZ-6, LCZ-8, and LCZ-10 showed positive departure. LCZ-A, LCZ-D, and LCZ-E showed positive departure, 4.45 °C, 1.72 °C, and 0.52 °C, respectively. LCZ-B and LCZ-G showed negative departure, about 0.49 °C and 2.16 °C in value, respectively.

The wintertime citywide average LST was 4.42 °C, and the wintertime departure pattern was similar to the autumntime one, despite different departure distance. In spring, the citywide average LST was 27.45 °C. LCZ-1, LCZ-4, and LCZ-4 showed negative departure with a value of 1.57 °C, 1.35 °C, and 0. 01 °C, respectively. LCZ-3, LCZ-8, and LCZ-10 showed obvious positive departure by 0.87 °C, 1.63 °C, and 0.55 °C, respectively. LCZ-A, LCZ-D, and LCZ-E exhibited positive departure by 2.51 °C, 0.90 °C, and 1.07 °C, respectively. Overall, the departure pattern of each zone generally varied with season. Even though, LCZ-3, LCZ-4, LCZ-8, LCZ-10, LCZ-A, and LCZ-E showed positive departure stably, and LCZ-B and LCZ-G showed stable positive and negative departure. Typically, LCZ-A (dense trees) was a strong warming zone.

D. Seasonal Variability of LCZ-Based LST in Nanjing

Fig. 9 shows the minimum, average, and maximum LST of each zone in Nanjing. Summertime, autumntime, wintertime, and springtime citywide LST ranged between 24.54 °C–49.85 °C, 8.38 °C–38.29 °C, −15.14 °C–20.39 °C, and 16.87 °C–39.47 °C, with the range of 25.31 °C, 29.91 °C, 35.53 °C, and 22.60 °C, respectively. The highest and lowest

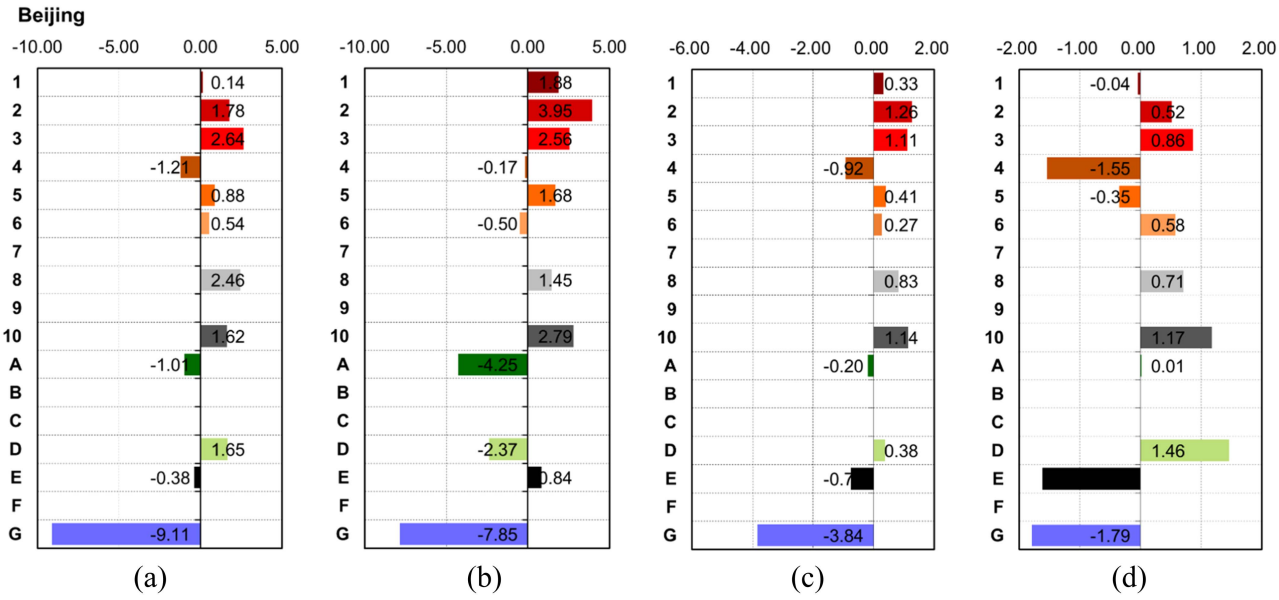

Fig. 6. Departure of LCZ-based LST from the average citywide LST in Beijing. (a) Spring. (b) Summer. (c) Autumn. (d) Winter.

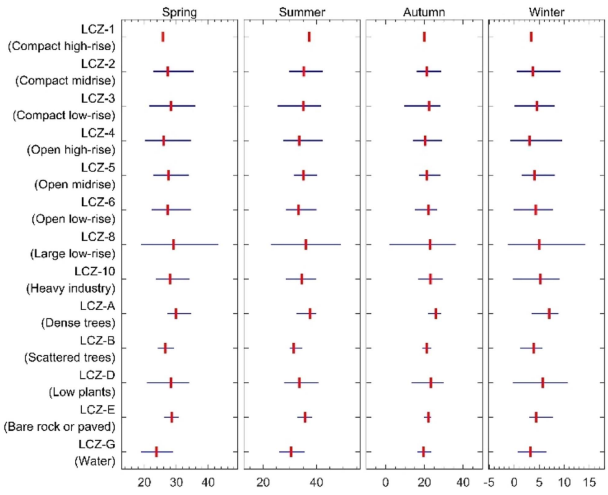

Fig. 7. Seasonal LST of different LCZs in Xi'an (°C). Note that the red dot was the average LST of each zone, and the left and right ends of the blue lines were the lowest and highest LSTs of each zone, respectively.

temperatures were found in LCZ-8 and LCZ-G in summer, LCZ-8 and LCZ-8 in autumn, LCZ-8 and LCZ-8 in winter, and LCZ-8 and LCZ-G in spring, respectively. The average LST ranged between 28.56 °C and 35.11 °C in summer. LCZ-G showed the lowest average temperature, while LCZ-3 showed the highest average temperature. In autumn, LCZ-G and LCZ-3 showed the lowest and highest average LST, with a value of 20.76 °C and 25.64 °C, respectively. LCZ-G and LCZ-3 had the lowest and highest average LST in winter, with a value of 6.06 °C and 8.41 °C, respectively. In spring, the average LST ranged between 21.57 °C and 28.08 °C, where LCZ-G and LCZ-3 covered two ends. Overall, LCZ-8 had the highest LST, while the zones with the highest average temperature was LCZ-3. LCZ-8 exhibited the lowest LST in spring, autumn, and winter, while LCZ-G showed the lowest average LST in four seasons.

The LST departure showed two key patterns (Fig. 10). In spring and summer, the citywide average LST were 33.02 °C and 26.36 °C, respectively. In spring, LCZ-1 and LCZ-4 showed negative departure of 0.40 °C and 0.74 °C, respectively. LCZ-A, LCZ-B, and LCZ-G showed negative departure of 0.87 °C, 0.40 °C, and 4.79 °C, respectively. However, in summer, all built-dominated zones were heating sources, where the LCZ-3 showed the strongest warming effect of 2.09 °C. LCZ-E and LCZ-F also exhibited warming effects by 0.21 °C and 0.75 °C, respectively.

The autumntime and wintertime citywide average LST were 24.08 °C and 7.41 °C, respectively. Their departure patterns were similar overall; the only difference was found in LCZ-E and LCZ-F. They exhibited warming effects in autumn with positive departure distance of 1.19 °C and 0.45 °C, respectively, whereas they were cooling zones in winter, with negative departure distance of 0.01 °C and 0.15 °C, respectively. Among built-dominated zones, LCZ-3, LCZ-8, and LCZ-10 exhibited warming effects, and their positive departure was 1.56 °C, 1.12 °C, and 0.95 °C in autumn, while it was 1.00 °C, 0.41 °C, and 0.95 °C, respectively. LCZ-1, LCZ-2, LCZ-4, LCZ-5, and LCZ-6 were cooling sources, with the LCZ-4 showed the strongest intensity in both autumn and winter. Among nonbuilt-dominated zones, LCZ-C showed prominent warming effects with the positive departure of 1.20 °C and 0.90 °C, in autumn and winter, respectively. LCZ-G was the most prominent cooling source with the negative departure of 3.32 °C and 1.35 °C in autumn and winter, respectively.

E. Seasonal Variability of LCZ-Based LST in Nanchang

Fig. 11 shows the mimimum, average, and maximum LST of Nanchang. The summertime, autumntime, wintertime, and springtime LST ranged from 21.80 °C–40.83 °C, 15.74 °C–39.93 °C, −6.42 °C–19.60 °C, and 5.01 °C–38.61 °C, resulting

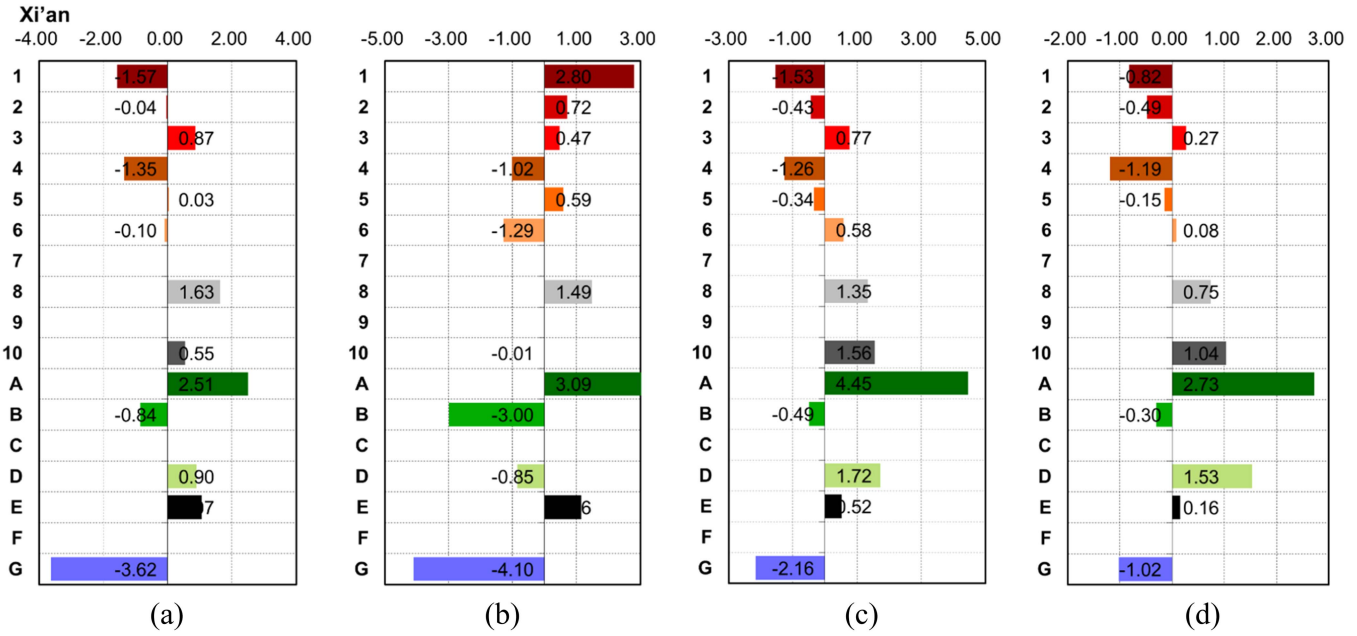

Fig. 8. Departure of LCZ-based LST from the average citywide LST in Xi'an. (a) Spring. (b) Summer. (c) Autumn. (d) Winter.

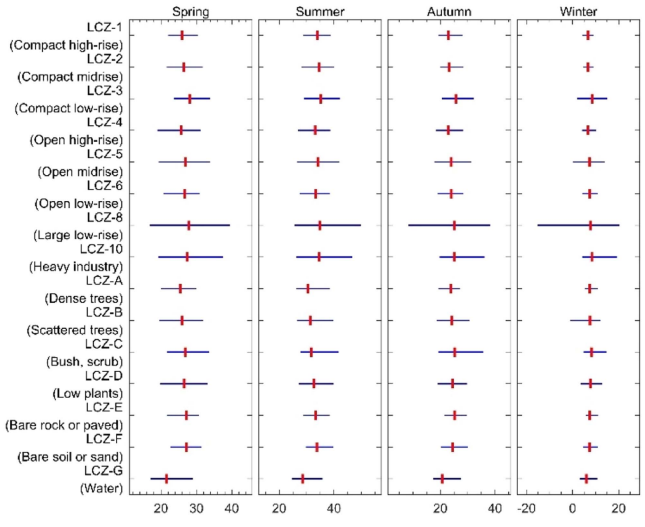

Fig. 9. Seasonal LST of different LCZs in Nanjing (°C). Note that the red dot was the average LST of each zone, and the left and right ends of the blue lines were the lowest and highest LSTs of each zone, respectively.

in a range of 19.03 °C, 24.19 °C, 26.02 °C, and 33.50 °C, respectively. The lowest and highest temperatures were found in LCZ-G and LCZ-8 in summer, LCZ-G and LCZ-8 in autumn, LCZ-A and LCZ-8 in winter, and LCZ-F and LCZ-8 in spring, respectively. In terms of average LST, LCZ-G and LCZ-8 showed the lowest and highest values in all four seasons, despite the differences in value.

Fig. 12 presents the seasonal temperature departure of Nanchang. Springtime, summertime, autumntime, and wintertime citywide average LSTs were 26.21 °C, 31.77 °C, 29.16 °C, and 9.84 °C, respectively. The temperature departure in spring, summer, and autumn showed a similar pattern, where only LCZ-A showed a different departure pattern among 14 zones. LCZ-A exhibited negative departure with a value of 0.02 °C and 0.09 °C in spring and winter, respectively, whereas it exhibited positive departure with a value of 0.13 °C in autumn.

Among built-dominated zones, LCZ-4 was the only one generating cooling effects in spring, summer, and autumn, with negative departure values of of 0.47 °C, 0.23 °C, and 0.39 °C, respectively. LCZ-8 exhibited the obvious positive departure, with values of 2.19 °C, 1.61 °C, and 1.46 °C in spring, summer, and autumn, respectively. In addition, LCZ-3 and LCZ-6 were built-dominated zones with prominent warming effects. Among nonbuilt-dominated zones, LCZ-E was the only one exerting a warming effect, with positive departure of 1.47 °C, 1.44 °C, and 0.97 °C in spring, summer, and autumn, respectively. LCZ-G was the most prominent cooling zone with the negative departure of 4.93 °C, 3.34 °C, and 3.69 °C in spring, summer, and autumn, respectively. In winter, LCZ-3, LCZ-6, and LCZ-8 showed positive departure, while LCZ-1, LCZ-2, LCZ-4, and LCZ-5 showed negative departure. LCZ-B, LCZ-C, and LCZ-E showed positive departure among seven nonbuilt-dominated zones, while LCZ-G showed obvious negative departure of 1.82 °C.

F. Seasonal Variability of Hot and Cold Zones of Five Megacities

Based on the analysis in subsections A–E, this subsection extracted the built-dominated and nonbuilt-dominated zones with high and low temperatures (e.g., type and occurrence time) in five megacities (Table III). This is crucial for urban planners, designers, and managers to identify the heat-prone and heat-safe zones in warm seasons and pinpoint the cold-prone and cold-safe

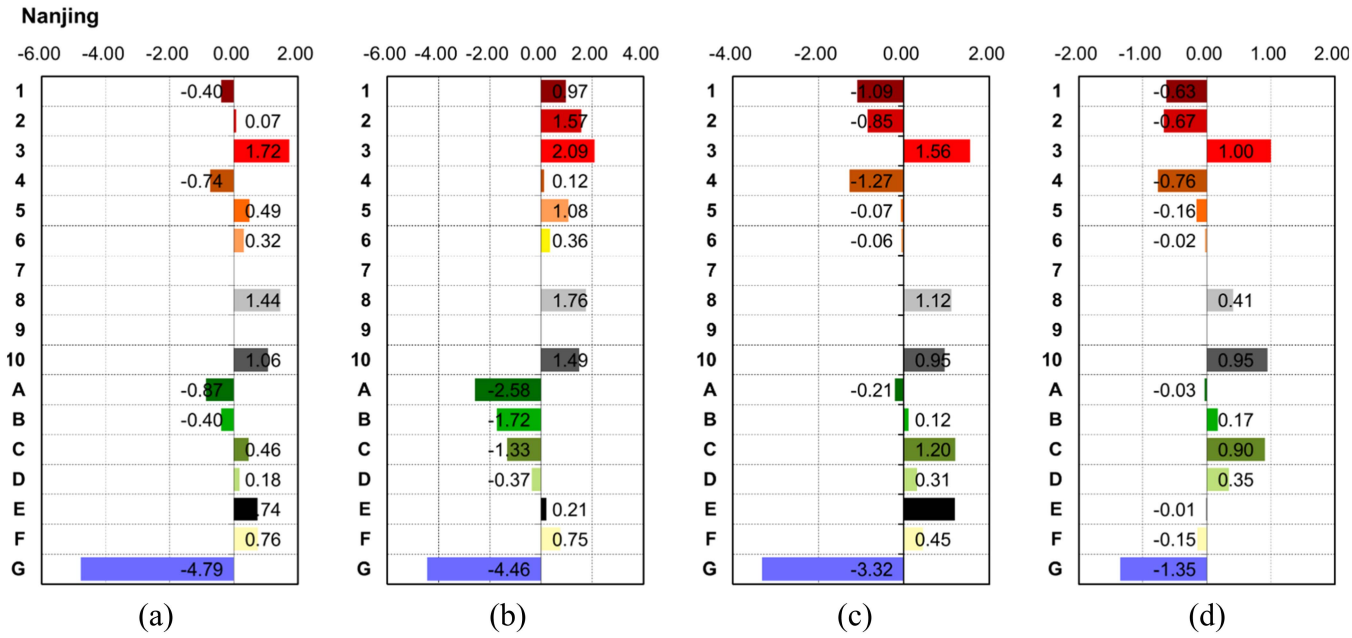

Fig. 10. Departure of LCZ-based LST from the average citywide LST in Nanjing. (a) Spring. (b) Summer. (c) Autumn. (d) Winter.

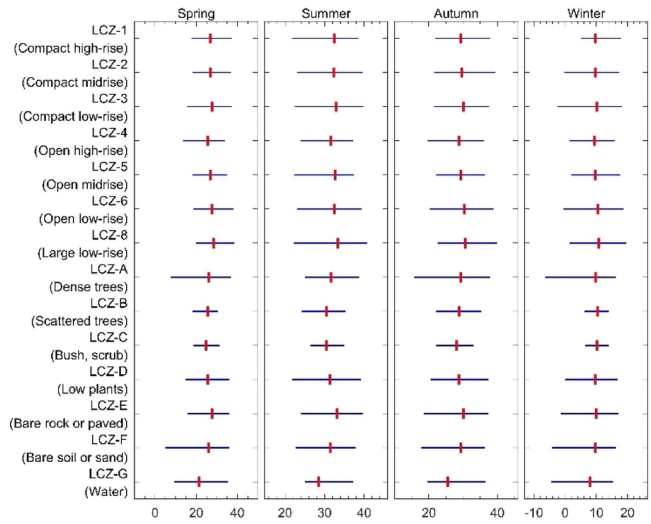

Fig. 11. Seasonal LST of different LCZs in Nanchang (°C). Note that the red dot was the average LST of each zone, and the left and right ends of the blue lines were the lowest and highest LSTs of each zone, respectively.

zones in cold seasons, for mitigation, adaptation, and governance interventions. Although the background temperatures in different years (e.g., 2016, 2017, 2018, 2019, and 2020) may cause some uncertainties in the seasonal variability of hot and cold zones, the results remained robust and reliable given the representative air temperatures of different seasons (Table I).

For the built-dominated zones in Shenyang, four zones were hot zones (i.e., including the hottest and hotter zones corresponding to the highest and second highest temperatures, respectively) in four seasons: LCZ-8, LCZ-2, LCZ-9, and LCZ-10 were the hottest zones of spring, summer, autumn, and winter, respectively. LCZ-8 was the hotter zone in summer and winter, and LCZ-10 was the hotter zone in spring and autumn. Four zones were identified as the cold zones (i.e., including the coldest and colder zones corresponding to the lowest and second lowest temperatures, respectively), where LCZ-4 and LCZ-1 were the coldest and colder zones in spring, autumn, and winter. LCZ-8 and LCZ-6 were identified as the coldest and colder zones of spring, respectively.

In Beijing, four zones were among the hottest and hotter built-dominated zones as well. LCZ-2 was the hottest zone in summer and autumn, while LCZ-3 and LCZ-10 were the hotter zones in spring and winter, respectively. LCZ-8 was the hotter zone in spring, LCZ-10 was the hotter zone in summer and autumn, and LCZ-3 was the hotter zone in winter. LCZ-2 was the hottest zone in summer and the hotter zone in autumn. LCZ-3 was the hottest one in spring. Four built-dominated zones were characterized by the coldest and colder zones in four seasons. LCZ-4 was the coldest in spring, autumn, and winter, and the colder one in summer. LCZ-1 was the colder zone in spring, LCZ-6 was the one in autumn, and LCZ-5 was the one in winter.

In Xi'an, there were four zones among the hottest and hotter zones. LCZ-8 was the hottest one in spring, and it was the hotter zone in summer, autumn, and winter. LCZ-7 was the hottest in summer, and LCZ-10 was the hottest in autumn and winter. LCZ-3 was the hotter zone in spring. LCZ-1 was the coldest zone in spring and autumn, LCZ-6 was the coldest zone in only summer, and LCZ-4 was the coldest zone in winter. However, LCZ-4 was the colder zone in spring, summer, and autumn, and LCZ-1 was the colder zone in winter. Typically, the pattern in autumn and winter was highly similar.

In Nanjing, LCZ-3 and LCZ-8 were the hottest and hotter zones in spring, summer, and autumn, while LCZ-3 and LCZ-10

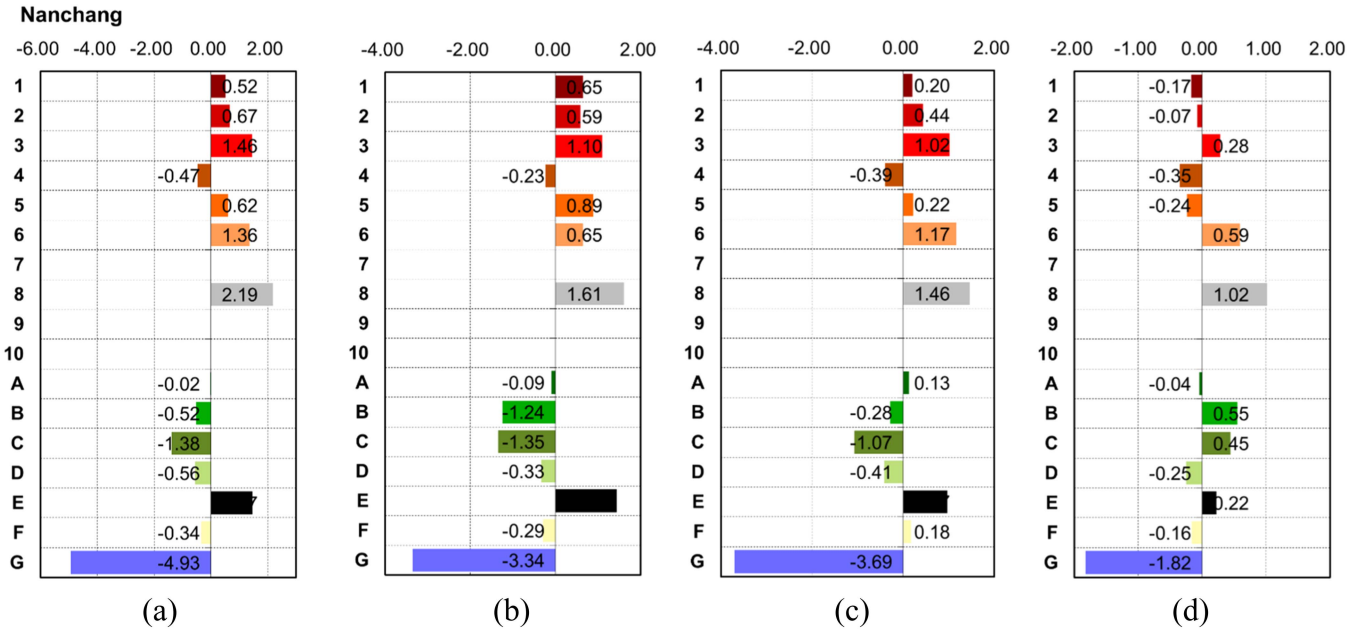

Fig. 12. Departure of LCZ-based LST from the average citywide LST in Nanchang. (a) Spring. (b) Summer. (c) Autumn. (d) Winter.

were the hottest and hotter zones in winter. LCZ-4 was always the coldest zone in all seasons. LCZ-1 was the colder in spring and autumn. LCZ-6 and LCZ-2 were colder in summer and winter, respectively.

In Nanchang, LCZ-8 was the hottest zone in four seasons. LCZ-3 was the hotter zone in spring and summer, while LCZ-6 was the hotter zone in autumn and winter. LCZ-4 was the coldest zone in all seasons, and LCZ-1 was the colder zone in spring and autumn. LCZ-2 and LCZ-5 were the colder zones in summer and winter, respectively.

The comparison indicates that the temperature pattern was not always the same in different seasons. As shown in Figs. 13 and 15 out of the 40 times, LCZ-8 (large low-rise) was the hottest/hotter zone, followed by LCZ-3 (nine times), LCZ-10 (six times), and LCZ-2 (three times). The respective values for LCZ-6 and LCZ-9 were only two and three times. In 19 out of 40 times, LCZ-4 (open high-rise), was the coldest/colder built-dominated zone, followed by LCZ-1 (11 times) and LCZ-6 (five times). The respective values for LCZ-2, LCZ-5, and LCZ-8 were only two, two, and one time. The seasonal temperature pattern was also different. For instance, there were three types of hot built-dominated zones in spring, while there were five in summer. In autumn and winter, there were six and four hot built-dominated zones, respectively. Moreover, the occurrence of different zones varied in four seasons. For instance, LCZ-8 occurred five, four, three, and three times in spring, summer, autumn, and winter, respectively. The cold built-dominated zones were also different in terms of type and associated occurrence time. For instance, LCZ-6 occurred four times in summer, while it was not a cold zone in both spring and winter.

Table III also presents the seasonal variability of hot and cold nonbuilt-dominated zones of different megacities. In Shenyang, LCZ-D, LCZ-E, and LCZ-F were the three hot nonbuilt-dominated zones. LCZ-F was the hottest zone in spring, and it was the hotter zone in summer, autumn, and winter. LCZ-E was the hottest in summer and autumn. LCZ-D was the coldest in winter, and the colder one in spring. LCZ-A and LCZ-G, representing dense trees and water, were the cold zones. LCZ-A was the coldest in summer, and the colder one in spring and autumn. LCZ-G was the coldest in spring and autumn and the colder one in summer and winter. In addition, LCZ-E was the coldest one in winter.

In Beijing, LCZ-A, LCZ-D, and LCZ-E were the three hot zones. LCZ-D was the hottest zone in spring, autumn, and winter, while it was the hotter one in summer. LCZ-E was the hottest zone in summer and the hotter zone in spring. LCZ-A, LCZ-E, and LCZ-G were the three cold zones. LCZ-G was the coldest one in the four seasons, and LCZ-A was the colder one in spring and summer. LCZ-E was the colder one in autumn and winter.

In Xi'an, there were three zones (e.g., LCZ-A, LCZ-D, and LCZ-E) characterized by hot zones. LCZ-A was the hottest in four seasons, LCZ-E was the hotter zone in spring and summer, and LCZ-D was the hotter zone in autumn and winter. LCZ-G and LCZ-B were the coldest and colder zones in the four seasons. Overall, spring and summer had the same pattern in terms of the hot and cold zones, while autumn and winter had the same pattern.

In Nanjing, there were four hot nonbuilt-dominated zones including LCZ-C, LCZ-D, LCZ-E, and LCZ-F. LCZ-F was the hottest zone in spring and summer, and LCZ-C was the hottest zone in autumn and winter. LCZ-E was the hotter one in spring, summer, and winter, while LCZ-D was the hotter one in winter. However, LCZ-G was the coldest zone in four seasons, and LCZ-A was the colder hotter one in four seasons except for winter. LCZ-F was the colder zone in winter. Overall, spring

TABLE III
SEASONAL VARIABILITY OF THE HOT AND COLD ZONES OF BUILT-DOMINATED AND NONBUILT-DOMINATED AREAS IN FIVE MEGACITIES (°C)

LCZ types	Megacities	Seasons	Max-1		Max-2		Min-1		Min-2	
Built-dominated	Shenyang	Spring	LCZ- 8	19.53	LCZ-10	19.13	LCZ-4	15.96	LCZ-1	16.49
		Summer	LCZ- 2	34.79	LCZ-8	34.24	LCZ-8	31.83	LCZ-6	31.87
		Autumn	LCZ- 9	21.77	LCZ-10	21.50	LCZ-4	19.71	LCZ-1	20.30
		Winter	LCZ- 10	-5.74	LCZ-8	-5.94	LCZ-4	-7.76	LCZ-1	-7.67
	Beijing	Spring	LCZ- 3	31.99	LCZ-8	31.81	LCZ-4	28.14	LCZ-1	29.49
		Summer	LCZ- 2	42.66	LCZ-10	41.50	LCZ-6	38.21	LCZ-4	38.54
		Autumn	LCZ- 2	21.09	LCZ-10	20.97	LCZ-4	18.91	LCZ-6	20.10
		Winter	LCZ- 10	2.79	LCZ-3	2.48	LCZ-4	0.07	LCZ-5	1.27
	Xi'an	Spring	LCZ- 8	29.08	LCZ-3	28.32	LCZ-1	25.88	LCZ-4	26.10
		Summer	LCZ- 7	37.32	LCZ-8	36.10	LCZ-6	33.23	LCZ-4	33.50
		Autumn	LCZ- 10	23.15	LCZ-8	22.94	LCZ-1	20.06	LCZ-4	20.33
		Winter	LCZ- 10	5.26	LCZ-8	4.97	LCZ-4	3.03	LCZ-1	3.40
	Nanjing	Spring	LCZ- 3	28.08	LCZ-8	27.80	LCZ-4	25.62	LCZ-1	25.96
		Summer	LCZ- 3	35.11	LCZ-8	34.78	LCZ-4	33.14	LCZ-6	33.38
		Autumn	LCZ- 3	25.64	LCZ-8	25.20	LCZ-4	22.81	LCZ-1	22.99
		Winter	LCZ- 3	8.41	LCZ-10	8.36	LCZ-4	6.65	LCZ-2	6.74
	Nanchang	Spring	LCZ- 8	28.40	LCZ-3	27.67	LCZ-4	25.74	LCZ-1	26.73
		Summer	LCZ- 8	33.38	LCZ-3	32.87	LCZ-4	31.54	LCZ-2	32.36
		Autumn	LCZ- 8	30.62	LCZ-6	30.33	LCZ-4	28.77	LCZ-1	29.36
		Winter	LCZ- 8	10.86	LCZ-6	10.43	LCZ-4	9.49	LCZ-5	9.50
Non-built-dominated	Shenyang	Spring	LCZ- F	19.49	LCZ-D	19.48	LCZ-G	14.18	LCZ-A	15.76
		Summer	LCZ- E	33.74	LCZ-F	31.08	LCZ-A	27.80	LCZ-G	28.18
		Autumn	LCZ- E	21.40	LCZ-F	21.26	LCZ-G	18.51	LCZ-A	19.46
		Winter	LCZ- D	-4.53	LCZ-F	-5.41	LCZ-E	-7.05	LCZ-G	-6.68
	Beijing	Spring	LCZ- D	31.00	LCZ-E	28.97	LCZ-G	20.24	LCZ-A	28.34
		Summer	LCZ- E	39.55	LCZ-D	36.34	LCZ-G	30.86	LCZ-A	34.46
		Autumn	LCZ- D	20.21	LCZ-A	19.63	LCZ-G	15.99	LCZ-E	19.07
		Winter	LCZ- D	3.08	LCZ-A	1.63	LCZ-G	-0.17	LCZ-E	0.00
	Xi'an	Spring	LCZ- A	29.96	LCZ-E	28.52	LCZ-G	23.83	LCZ-B	26.61
		Summer	LCZ- A	37.61	LCZ-E	35.68	LCZ-G	30.42	LCZ-B	31.52
		Autumn	LCZ- A	26.04	LCZ-D	23.31	LCZ-G	19.43	LCZ-B	21.10
		Winter	LCZ- A	6.95	LCZ-D	5.75	LCZ-G	3.20	LCZ-B	3.92
	Nanjing	Spring	LCZ- F	27.12	LCZ-E	27.10	LCZ-G	21.57	LCZ-A	25.49
		Summer	LCZ- F	33.77	LCZ-E	33.23	LCZ-G	28.56	LCZ-A	30.44
		Autumn	LCZ- C	25.28	LCZ-E	25.27	LCZ-G	20.76	LCZ-A	23.87
		Winter	LCZ- C	8.31	LCZ-D	7.76	LCZ-G	6.06	LCZ-F	7.26
	Nanchang	Spring	LCZ- E	27.68	LCZ-A	26.19	LCZ-G	21.28	LCZ-C	24.83
		Summer	LCZ- E	33.21	LCZ-A	31.68	LCZ-G	28.43	LCZ-C	30.42
		Autumn	LCZ- E	30.13	LCZ-F	29.34	LCZ-G	25.47	LCZ-C	28.09
		Winter	LCZ- B	10.39	LCZ-C	10.29	LCZ-G	8.02	LCZ-D	9.59

Note: For both built-dominated and nonbuilt-dominated zones, Max-1 and Max-2 were their highest and the second highest temperature among all possible zones, respectively; and Min-1 and Min-2 were the lowest and the second lowest temperature among all possible zones, respectively.

and summer had the same pattern in terms of the hot and cold zones.

In Nanchang, LCZ-A, LCZ-B, LCZ-C, LCZ-E, and LCZ-F were the hot nonbuilt-dominated zones. LCZ-E was the hottest in spring, summer, and autumn, while LCZ-B was the hottest in winter. LCZ-A was the hotter one in spring and summer, LCZ-F was the hotter one in autumn, and LCZ-C was the hotter one in winter. Regarding the cold zones, LCZ-G, representing low plants and water, was the coldest one in all seasons. LCZ-C was the colder zone in spring, summer, and autumn, while LCZ-D was the colder zone in winter. Overall, the analysis indicates that both hot and cold nonbuilt-dominated zones varied significantly with city and season. Some zones were the hottest in one season, but changed to be the coldest in another season. For instance, in Shenyang, LCZ-8 was the hottest one in spring, while it was the coldest one in summer; LCZ-E was the hottest one in summer and autumn, while it was the coldest one in winter. Some sharp changes were also found in specific zones in terms of being hotter and colder zones in different seasons.

Fig. 13 also presents the characteristic hot and cold zones in five megacities. LCZ-E (bare rock or paved) was a typical hot nonbuilt-dominated zone with 12 times of occurrence, followed by LCZ-D (nine times), LCZ-A (eight times), and LCZ-F (seven times). LCZ-B and LCZ-C occurred one and three times, respectively. LCZ-G (water) was the most typical cold nonbuilt-dominated zone with 20 times of occurrence, followed by LCZ-A (dense trees) with eight times. LCZ-B, LCZ-C, LCZ-D, LCZ-E, and LCZ-F occurred four, three, one, three, and one time, respectively. The hot and cold nonbuilt-dominated zones varied significantly in different seasons as well. For instance, four, four, five, and five zones were hot zones in spring, summer, autumn, and winter, respectively. Four, four, five, and five zones were cold zones in spring, summer, autumn, and winter. Overall, there were no fixed hot and cold zones in different seasons.

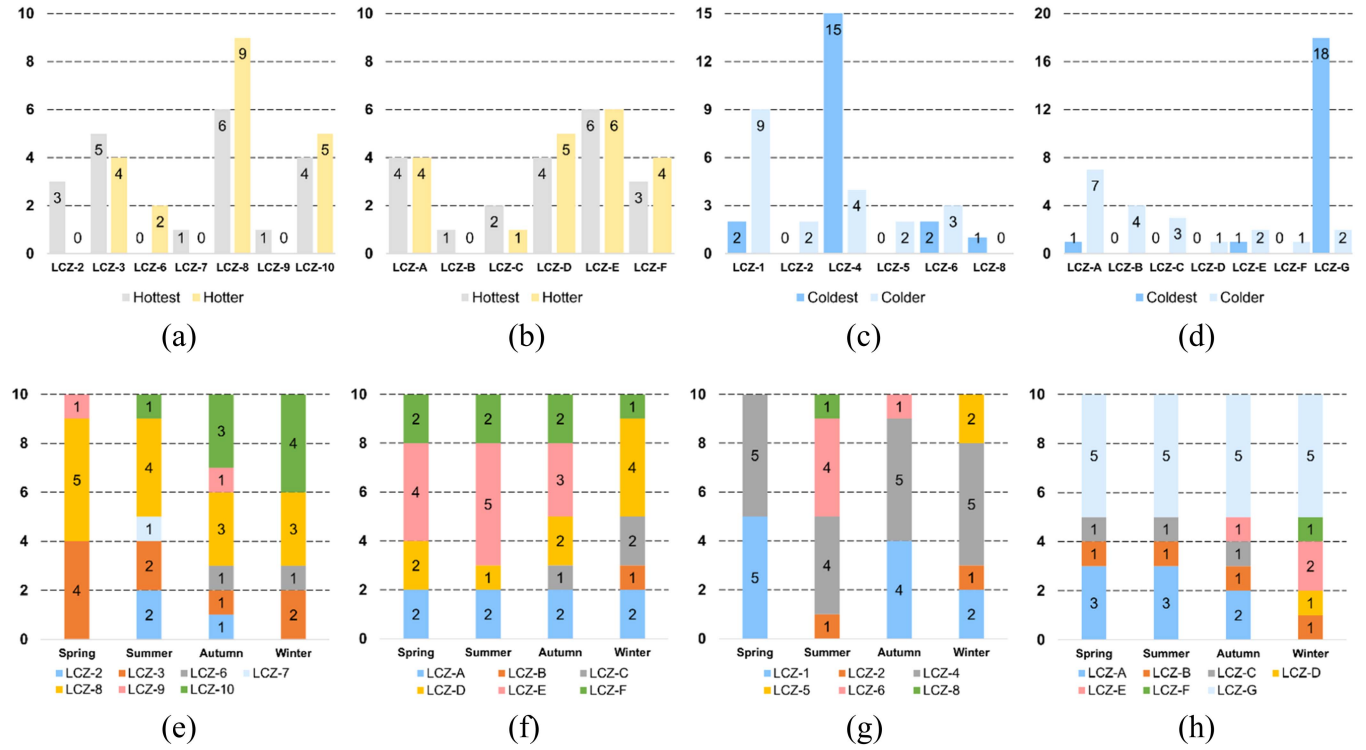

Fig. 13. Characteristic hot and cold zones in built-dominated and nonbuilt-dominated zones. Note the hottest and hotter zones were the zones with the highest (Max-1) and the second highest temperatures (Max-2) in Table III, and the coldest and colder zones were those with the lowest (Min-1) and the second lowest temperatures (Min-2). (a) Hot built-dominated zones. (b) Hot non-built-dominated zones. (c) Cold built-dominated zones. (d) Cold non-built-dominated zones. (e) Hot built-dominated zones. (f) Hot non-built-dominated zones. (g) Cold built-dominated zones. (h) Cold non-built-dominated zones.

G. Land Surface Temperature Difference Among Different Local Climate Zones

Fig. 14 compares whether there was a significant difference between the temperatures of pairwise LCZs. The results indicate that the temperatures of most pairwise built-dominated and nonbuilt-dominated zones showed significant differences. However, many pairwise zones did not show significant differences. Among the built-dominated zone of Shenyang, for instance, the temperature of LCZ-2 did not have a significant difference from that of LCZ-6, and there was no significant difference between the temperatures of LCZ-3 and LCZ-10 in spring. In summer, LCZ-3 did not significantly differ from those of LCZ-5 and LCZ-10 in temperature. In autumn, the temperature of LCZ-2 was not significantly different from those of LCZ-3 and LCZ-10. In winter, the temperature of LCZ-3 was not significantly different from those of LCZ-6 and LCZ-10. Among nonbuilt-dominanted zones in Shenyang, only temperatures of a few pairwise zones showed significant differences. The number of significantly different pairwise LCZs was 10, 11, 11, and 11 in spring, summer, autumn, and winter, respectively. Overall, the LCZ scheme's capability to differentiate LST was not always robust.

Among the built-dominated zones in Beijing, many pairwise LCZs showed significant differences in LST in spring, summer, autumn, winter, showing a more robust LCZ scheme capability than that in Shenyang. However, compared with Shenyang, fewer pairwise nonbuilt-dominated zones showed significant differences. There were three, one, two, and four pairs in spring, summer, autumn, and winter, respectively. In Xi'an, LCZ-2 showed no significant differences from LCZ-5 and LCZ-6 in spring. The LCZ scheme's capability to differentiate the LST of nonbuilt-dominated zones was not very robust, especially in spring, summer, and winter. In Nanjing, LCZ scheme's capability to characterize the LST of built-dominated zones was overall good, and its capability to characterize the LST of nonbuilt-dominated zones was better than those in Shenyang, Beijing, and Xi'an. In Nanchang, the LCZ scheme's capability to differentiate the LST of built-dominated zones was overall good, and it was much better in spring, autumn, and winter than that in summer. Overall, the capability to differentiate the LST of nonbuilt-dominated zones was weaker.

Fig. 15 shows the LCZ scheme's capability to differentiate LST of builtdominated and nonbuilt-dominated zones in terms of difference level, which is the ratio of pairwise LCZs with significantly different temperatures to all pairwise LCZs. In Shenyang, the LCZ scheme's capability to differentiate the temperatures of built-dominated zones overall exceeded 80%. The best capability among built-dominated zones was found in spring, about 92.86%, and it was only 82.14% in both summer and winter. The capability among nonbuilt-dominated zones ranged only between 66.67% and 73.33%. In Beijing, the LCZ scheme's capability among built-dominated zones was high, ranging between 89.29% and 96.43%, while it was only between

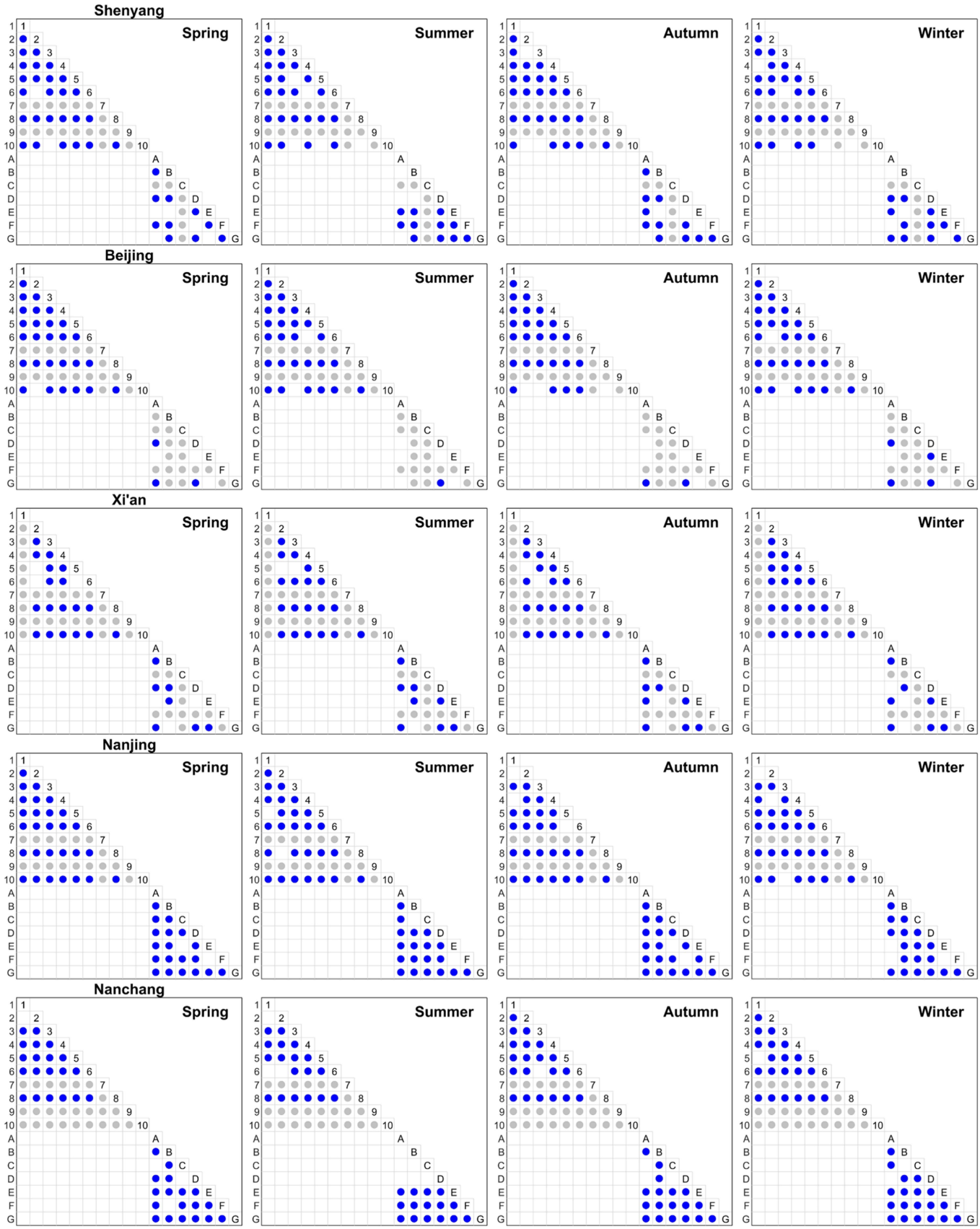

Fig. 14. Difference of land surface temperatures of different LCZ types (blue dots denote significant difference at $p < 0.05$ level, grey dots denote no comparison, and blank dots denote no significant difference).

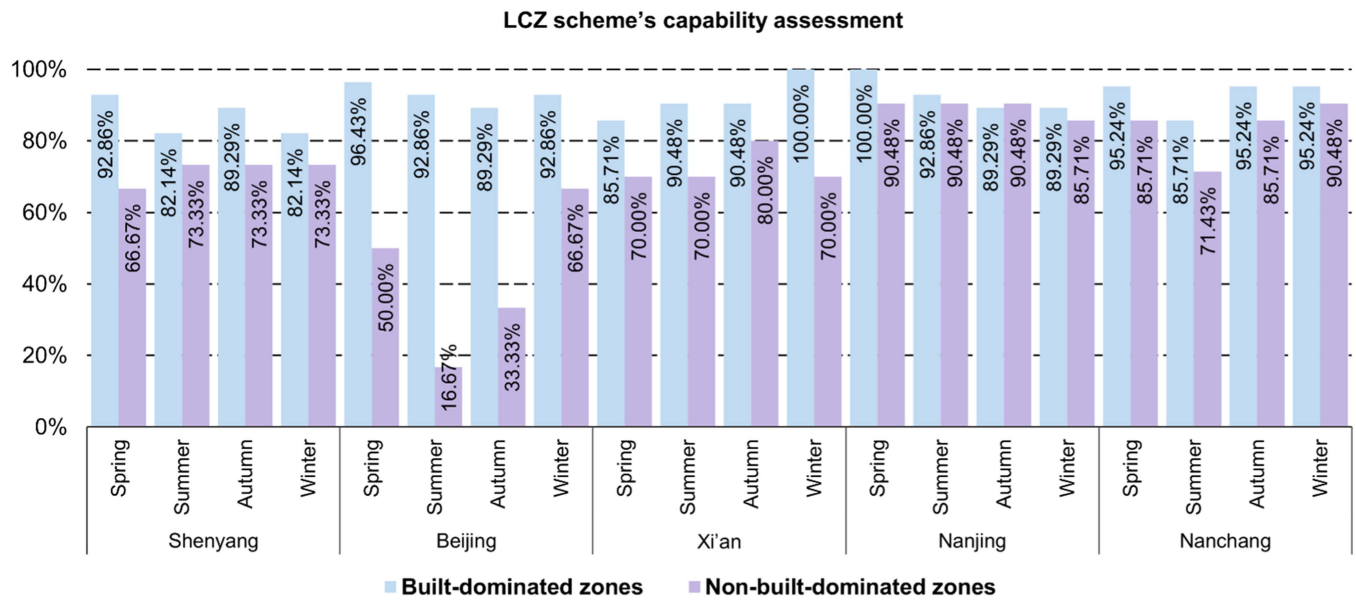

Fig. 15. Assessment of LCZ scheme's capability to differentiate land surface temperatures.

16.67% and 66.67% among nonbuilt-dominated zones. In Xi'an, LCZ scheme's capability ranged between 86.71% and 100% among built-dominated zones, and it was between 70% and 80% among nonbuilt-dominated zones. In Nanjing, LCZ scheme's capability among built-dominated zones exceeded 85% in four seasons, with the highest level being 100% in spring. The capability among nonbuilt-dominated zones ranged between 85.71% and 90.48%.

In Nanchang, among built-domianted zones, the capability was 95.24% in spring, autumn, and winter, followed by 85.71% in summer. Among nonbuilt-dominated zones, the capability level varied, and it was 71.43% in summer. Overall, this article proved the seasonal variations of LCZ scheme's capacity. However, there might be some uncertainties caused by the mismatched years of LCZ and LST data. It is essential to further control the same year for original data production for better verification.

IV. Implications for Heat-Resilient Planning and Design

Cities are affected by increasingly frequent, severe, and intense urban heat challenges. Integrating heat resilience into cities and communities through mitigation, adaptation, and management solutions is important to protect urban dwellers [37], [38]. This, to a large extent, depends on the understanding of urban morphological characteristics. LCZ scheme shows its advantage in standardizing urban morphological characteristics by respecting morphological homogeneity and heterogeneity. The LCZ scheme demonstrates its potential to be integrated into heat-resilient planning and design. However, the reliability and robustness of integrating LCZ scheme into heat-resilient planning and design has not been well documented. This article investigated LCZ scheme's capability to differentiate the LST of five megacities in China and generated some implications for heat-resilient planning and design.

Assessment of heat risks is critical to identify hot and cold spots, as well as heat risky areas. First, at the city scale, the LST showed a large temperature range across four seasons in all five megacities. However, when using LCZ scheme to characterize the LST, the LCZ scheme only exhibited average LSTs of each zone with a smaller range at the local scale. As a result, the riskiest areas were ignored. Moreover, the LCZs with the most critical heat risks were also different from the zones with the highest average temperatures. This means the application of LCZ covers up the riskiest zones. Second, for heat mitigation, highlighting the principle of urban scale by implementing "city–local" heat identification method, is conducive to avoiding the average–induced errors, for accurately identifying the hottest patches for interventions. Nevertheless, the LCZ scheme is applicable for recognizing large zones for mitigation campaigns. Third, cold spots generally exhibit cold island effects so that they are conducive to better adaptive capacity in summer. For example, the low average temperatures of some zones overall represent the cold areas for adaptation, but the coldest spots might be overlooked when using the LCZ scheme. Moreover, there is a need to recognize the large temperature range of specific zones, which, to some extent, means the inclusion of extreme heat patches. This is particularly important for zones with cold island effects, when making adaptation and management decisions. Overall, the adoption of LCZ scheme is associated with the use of heat assessment indicators (e.g., minimum LST, maximum LST, average LST, and magnitude), urban scale (e.g., city and local), and spatial resolution for transformation.

According to the temperature departure pattern, it is found that whether a built-dominated zone contributed to urban temperature increase depended. The nonbuilt-dominated zones' contribution to urban temperature decrease also depended. Compact high-rise, compact midrise, and many others were not always the hottest zones [26]. Large low-rise and compact low-rise could also be hot zones. The nonbuilt-dominated could also

significantly contribute to an increase in urban temperature. For instance, bare rock or paved and bare soil or sand could also be hot zones and their temperatures could be higher than some built-dominated zones. In winter, compact high-rise and open high-rise could have the lowest temperatures in many cities [32]. Therefore, in heat-resilient urban planning and design, it is essential to accurately identify the most critical zones for implementing mitigation measures in specific city contexts.

Seasonal variation suggests that it is essential to control source data time seriously to avoid errors during heat risk assessment. The replacement of source data for summertime heat risk assessment with autumn data can result in significant biases. Some open spaces, such as bare rock, soil, and sand areas are not suggested for heat adaptation. Dense trees and water zones are mostly the cold zones, but this is not always true, according to the analysis. Open high-rise areas were cooler than many other built-dominated zones for heat adaptation. Apart from heat-related issues in summer, cold-related problems in winter are also temperature-related issues. Therefore, improving urban thermal quality by elevating the temperature of wintertime cold zones is also critical. During the process, there is a need to coordinate the mitigation of high temperatures of summertime hot zones and the mitigation of low temperatures of wintertime cold zones, especially for cities like Shenyang, Beijing, and Xi'an.

One of the advantages of LCZ is to differentiate urban temperatures. The results, however, indicate that not all LCZs showed significant differences in temperature from others. In Shenyang, LCZ scehme's capability among built-dominated zones was around 90% in four seasons, while the LCZ scheme's capability in Beijing was lower than 70% among nonbuilt-dominated zones. In heat–resilient urban planning and design, urban planners, designers, and managers should prudently adopt LCZ scheme to rank the priorities for integrating cooling interventions in both built-dominated and nonbuilt-dominated zones. It is important to not copy the LCZ-based LST pattern of other cities or seasons when making decisions.

V. Conclusion

LCZ classification scheme is a classic model to standardize urban surface cover and structure, making important contributions to understanding urban climate and variability. However, limited studies have examined its capability to differentiate urban temperatures and its reliability to inform heat-resilient urban planning and design. Through the analysis of five megacities in China, this article indicated that averaged surface temperatures of LCZs might result in overlooking the hot spots that exhibit critical heat-related risks. Meanwhile, the zones with hot spots could be covered up. The occurrence of hot and cold zones varied with urban and seasonal contexts. LCZ-8 was the typical hot zone in five megacities, but it was not stable, where LCZ-2, LCZ-3, LCZ-6, LCZ-7, and LCZ-10 could be hot zones as well. Nonbuilt-dominated zones were not always cold zones and they could have higher temperatures than built-dominated zones. Likewise, built-dominated zones were not always hot zones. Indeed, some built-dominated zones could contribute to urban temperature decrease in summer, and some nonbuilt-dominated zones made contributions to urban temperature increase. LCZ-E was a typical hot zone among nonbuilt-dominated zones, while LCZ-A, LCZ-B, LCZ-C, LCZ-D, and LCZ-F could be hot zones as well. LCZ-A and LCZ-G were typical cold zones, while some other LCZs could be cold zones as well. The LCZ scheme's ability to characterize urban temperatures of built-dominated zone was not always reliable, especially in Shenyang, Beijing, and Xi'an. The LCZ scheme had a higher capability to differentiate the temperatures of built-dominated zones, compared with nonbuilt-dominated zones. In summary, the integration of LCZ scheme into heat-resilient urban planning and design, in alignment with the city and seasonal variability of LCZ-based LST, should be tailored to city and seasonal contexts.

References

[1] D. Li and E. Bou-Zeid, "Synergistic interactions between urban heat islands and heat waves: The impact in cities is larger than the sum of its parts," *J. Appl. Meteorol. Climatol.*, vol. 52, no. 9, pp. 2051–2064, 2013.

[2] B. J. He et al., "Localized synergies between heat waves and urban heat islands: Implications on human thermal comfort and urban heat management," *Environ. Res.*, vol. 193, 2021, Art. no. 110584.

[3] B. Stone, *The City and the Coming Climate: Climate change in the Places We Live*. Cambridge, U.K., MA, USA: Cambridge Univ. Press, 2012.

[4] S. Adams et al., *Turn Down the Heat: Confronting the New Climate Normal*. Washington, DC, USA: The World Bank, 2014.

[5] Y. Cui, M. Yin, X. Cheng, J. Tang, and B.-J. He, "Towards cool cities and communities: Preparing for an increasingly hot future by the development of heat-resilient infrastructure and urban heat management plan," *Environ. Technol. Innov.*, vol. 34, 2024, Art. no. 103568.

[6] T. C. Lim, B. Wilson, J. R. Grohs, and T. J. Pingel, "Community-engaged heat resilience planning: Lessons from a youth smart city STEM program," *Landscape Urban Plan.*, vol. 226, 2022, Art. no. 104497.

[7] Y. Zhang and J. Cheng, "Spatio-temporal analysis of urban heat island using multisource remote sensing data: A case study in Hangzhou, China," *IEEE J. Sel. Topics Appl. Earth Observ. Remote Sens.*, vol. 12, no. 9, pp. 3317–3326, Sep. 2019.

[8] W. Liao, T. Hong, and Y. Heo, "The effect of spatial heterogeneity in urban morphology on surface urban heat islands," *Energy Buildings*, vol. 244, 2021, Art. no. 111027.

[9] M. Liu, H. Ma, and Y. Bai, "Understanding the drivers of land surface temperature based on multisource data: A spatial econometric perspective," *IEEE J. Sel. Topics Appl. Earth Observ. Remote Sens.*, vol. 14, pp. 12263–12272, 2021.

[10] D. Han et al., "The roles of surrounding 2D/3D landscapes in park cooling effect: Analysis from extreme hot and normal weather perspectives," *Building Environ.*, vol. 231, 2023, Art. no. 110053.

[11] D. Han et al., "Understanding the role of urban features in land surface temperature at the block scale: A diurnal cycle perspective," *Sustain. Cities Soc.*, vol. 10, 2024, Art. no. 105588.

[12] B. Yuan, L. Zhou, F. Hu, and C. Wei, "Effects of 2D/3D urban morphology on land surface temperature: Contribution, response, and interaction," *Urban Climate*, vol. 53, 2024, Art. no. 101791.

[13] J. Qi, L. Ding, and S. Lim, "Application of a decision-making framework for multi-objective optimisation of urban heat mitigation strategies," *Urban Climate*, vol. 47, 2023, Art. no. 101372.

[14] J. Qi, L. Ding, and S. Lim, "Planning for cooler cities: A framework to support the selection of urban heat mitigation techniques," *J. Cleaner Prod.*, vol. 275, 2020, Art. no. 122903.

[15] B.-J. He, L. Ding, and D. Prasad, "Relationships among local-scale urban morphology, urban ventilation, urban heat island and outdoor thermal comfort under sea breeze influence," *Sustain. Cities Soc.*, vol. 60, 2020, Art. no. 102289.

[16] B.-J. He, L. Ding, and D. Prasad, "Urban ventilation and its potential for local warming mitigation: A field experiment in an open low-rise gridiron precinct," *Sustain. Cities Soc.*, vol. 55, 2020, Art. no. 102028.

[17] Z. Wu, Y. Shi, L. Ren, and J. Hang, "Scaled outdoor experiments to assess impacts of tree evapotranspiration and shading on microclimates and energy fluxes in 2D street canyons," *Sustain. Cities Soc.*, vol. 108, 2024, Art. no. 105486.
[18] E. R. Lotfy, "Modelling of solar insolation on arrayed buildings with shading effect considered," *Sādhanā*, vol. 49, no. 2, pp. 1–16, 2024.
[19] B.-J. He, L. Ding, and D. Prasad, "Enhancing urban ventilation performance through the development of precinct ventilation zones: A case study based on the Greater Sydney, Australia," *Sustain. Cities Soc.*, vol. 47, 2019, Art. no. 101472.
[20] Y. Chen, J. Yang, W. Yu, J. Ren, X. Xiao, and J. Xia, "Relationship between urban spatial form and seasonal land surface temperature under different grid scales," *Sustain. Cities Soc.*, vol. 89, 2023, Art. no. 104374.
[21] Y. Chen, J. Yang, R. Yang, X. Xiao, and J. Xia, "Contribution of urban functional zones to the spatial distribution of urban thermal environment," *Building Environ.*, vol. 216, 2022, Art. no. 109000.
[22] A. Kafy et al., "Remote sensing-based approach to identify the influence of land use/land cover change on the urban thermal environment: A case study in Chattogram City, Bangladesh," in *Re-Envisioning Remote Sensing Applications*. Boca Raton, FL, USA: CRC Press, 2021, pp. 217–240.
[23] J. Ren, J. Yang, F. Wu, W. Sun, X. Xiao, and J. Xia, "Regional thermal environment changes: Integration of satellite data and land use/land cover," *Iscience*, vol. 26, no. 2, 2023, Art. no. 105820.
[24] Z.-Q. Zhao, B.-J. He, L.-G. Li, H.-B. Wang, and A. Darko, "Profile and concentric zonal analysis of relationships between land use/land cover and land surface temperature: Case study of Shenyang, China," *Energy Buildings*, vol. 155, pp. 282–295, 2017.
[25] B.-J. He, Z.-Q. Zhao, L.-D. Shen, H.-B. Wang, and L.-G. Li, "An approach to examining performances of cool/hot sources in mitigating/enhancing land surface temperature under different temperature backgrounds based on landsat 8 image," *Sustain. Cities Soc.*, vol. 44, pp. 416–427, 2019.
[26] I. D. Stewart, D. Ian, and T. R. Oke, "Local climate zones for urban temperature studies," *Bull. Amer. Meteorological Soc.*, vol. 93, no. 12, pp. 1879–1900, 2012.
[27] B. Bechtel and C. Daneke, "Classification of local climate zones based on multiple Earth observation data," *IEEE J. Sel. Topics Appl. Earth Observ. Remote Sens.*, vol. 5, no. 4, pp. 1191–1202, Aug. 2012.
[28] B. Rousse, S. Lobry, G. Duthé, V. Golaz, and L. Wendling, "Domain adaptation for mapping LCZs in Sub-Saharan Africa with remote sensing: A comprehensive approach to health data analysis," *IEEE J. Sel. Topics Appl. Earth Observ. Remote Sens.*, vol. 17, pp. 13016–13029, 2024.
[29] J. Yang, Y. Wang, C. Xiu, X. Xiao, J. Xia, and C. Jin, "Optimizing local climate zones to mitigate urban heat island effect in human settlements," *J. Cleaner Prod.*, vol. 275, 2020, Art. no. 123767.
[30] H. Zhang et al., "Application and future of local climate zone system in urban climate assessment and planning—Bibliometrics and meta-analysis," *Cities*, vol. 150, 2024, Art. no. 104999.
[31] J. Geletič, M. Lehnert, S. Savić, and D. Milošević, "Inter-/intra-zonal seasonal variability of the surface urban heat island based on local climate zones in three central European cities," *Building Environ.*, vol. 156, pp. 21–32, 2019.
[32] Z. Zhao, A. Sharifi, X. Dong, L. Shen, and B.-J. He, "Spatial variability and temporal heterogeneity of surface urban heat island patterns and the suitability of local climate zones for land surface temperature characterization," *Remote Sens.*, vol. 13, no. 21, 2021, Art. no. 4338.
[33] M. Žgela, I. Herceg-Bulić, J. Lozuk, and P. Jureša, "Linking land surface temperature and local climate zones in nine Croatian cities," *Urban Climate*, vol. 54, 2024, Art. no. 101842.
[34] J. R. Dymond, P. R. Stephens, P. F. Newsome, and R. H. Wilde, "Percentage vegetation cover of a degrading rangeland from SPOT," *Int. J. Remote Sens.*, vol. 13, no. 11, pp. 1999–2007, 1992.
[35] L. Guanter, M. Del Carmen González-Sanpedro, and J. Moreno, "A method for the atmospheric correction of ENVISAT/MERIS data over land targets," *Int. J. Remote Sens.*, vol. 28, no. 3/4, pp. 709–728, 2007.
[36] J. Ching et al., "WUDAPT: An urban weather, climate, and environmental modeling infrastructure for the anthropocene," *Bull. Amer. Meteorological Soc.*, vol. 99, no. 9, pp. 1907–1924, 2018.
[37] K. Xiong and B.-J. He, "Planning for heat-resilient educational precincts: Framework formulation, cooling infrastructure selection and walkable routes determination," *Sustain. Cities Soc.*, vol. 101, 2024, Art. no. 105183.
[38] B. Huang, X. Dong, Y. Tian, M. Yin, Y. Qiu, and B.-J. He, "Experimental investigation of the thermal usability of outdoor environments in rideability, walkability, entertainmentability, exercisability and workability for urban heat mitigation, adaptation and governance," *Natural Hazards*, vol. 120, no. 2, pp. 2005–2034, 2024.

Bao-Jie He received the Ph.D. degree in built environment from the University of New South Wales, NSW, Australia, in 2020.

He is currently a Full Professor of Urban Climate and Sustainable Built Environment with the Chongqing University, Chongqing, China. Prior to this, he worked with the University of New South Wales, Sydney, NSW, Australia. He is also the leader of Centre for Climate-Resilient and Low-Carbon Cities, Chongqing University, an Adjunct Associate Professor with the Queensland University, Brisbane, QLD, Australia, and the Honorary Research Fellow of the Hiroshima University, Hiroshima, Japan.

Xuecheng Fu received the B.Sc. degree in geographic information science and the M.Sc. degree in cartography and geographic information systems from the Shandong Normal University, Jinan, China, in 2020 and 2023, respectively. He is currently working toward the Ph.D. degree in architecture with the Chongqing University, Chongqing, China, under the supervision of Prof. Bao-Jie He.

His research interests include urban ecology and sustainable built environments.

Mr. Fu is a student member of the Geographical Society of China and the Ecological Society of China.

Ziqi Zhao received the B.Sc. degree in meteorology from the Shenyang Agricultural University, Shenyang, China, in 2011.

She is currently a Research Associate with the Institute of Atmospheric Environment, China Meteorological Administration, Shenyang, China. She has authoredcoauthored more than 10 papers in relevant fields. Her research interests include urban microclimate and urban thermal environments.

Pengxin Chen received the graduate degree in computer science and technology from the Shenyang University of Technology, Shenyang, China, in 2013.

He is employed by the Shenyang Meteorological Service, Liaoning Province. He is currently an Engineer who primarily engages in meteorological information and technology work, specializing in the development of meteorological software and information systems.

Ayyoob Sharifi received the Ph.D. degree in environmental engineering and architecture from Nagoya University, Japan, in 2013. He is currently a Professor with the IDEC Institute, Hiroshima University, Hiroshima, Japan.

He also has cross-appointments with the Graduate School of Humanities and Social Sciences and the Graduate School of Advances Science and Engineering. He actively contributes to global change research programs, such as the Future Earth and has served as a lead author for the Sixth Assessment Report of the Intergovernmental Panel on Climate Change. Before joining the Hiroshima University, he was the Executive Director of the Global Carbon Project, leading the urban flagship activity of the project. His research interests include interface of urbanism and climate change mitigation and adaptation. His research interests also include interface of climate change and urban planning. The ultimate goal of his research is to provide further insights into how to develop sustainable, peaceful, just, and resilient communities.

Hong Li received the Ph.D. degree in ecology from the Fudan University, Shanghai, China, in 2019.

She completed postdoctoral work with the University of Quebec at Montreal, Montreal, QC, Canada (2019–2021). She is currently an Assistant Professor with the Chongqing University, Chongqing, China. She has been focusing on studying LUCC and climate change based on experiments and data mining, since 2012.